FUSION ENGINEERING PHYSICS
Erasmus Mundus Joint Master Degree

European Master of Science in Nuclear Fusion and Engineering Physics

New Set of Inner Magnetic Coils at the GOLEM Tokamak

Master Thesis
presented by

Godsfavour Chibueze Amanekwe

Thesis Supervisor

RNDr. Jana Brotánková, Ph.D.
Faculty of Nuclear Physics and Physical Engineering
Czech Technical University in Prague

September 24, 2024

UNIVERSITEIT GENT
Universität Stuttgart
instn
uc3m Universidad Carlos III de Madrid
CTU CZECH TECHNICAL UNIVERSITY IN PRAGUE
UNIVERSITÉ DE LORRAINE
Aix*Marseille université Initiative d'excellence
UNIVERSIDAD COMPLUTENSE MADRID

New Set of Inner Magnetic Coils at the GOLEM Tokamak

Master Thesis
presented by

Godsfavour Chibueze Amanekwe

Thesis Supervisor

RNDr. Jana Brotánková, Ph.D.
Faculty of Nuclear Physics and Physical Engineering
Czech Technical University in Prague

Erasmus Mundus Program on Nuclear Fusion Science and Engineering Physics

September 24, 2024

Abstract

Systems of magnetic diagnostics belong to the backbones of magnetic confinement fusion devices. The GOLEM tokamak has as a part of the control system a Rogowski coil for the plasma current measurement, and a small coil for the toroidal field measurement, both outside the vacuum chamber.

A new system of magnetic coils was recently developed and installed inside the GOLEM vacuum vessel. The system consists of a Rogowski coil, two toroidal field coils placed on the high field side (HFS) and the low field side (LFS), and a diamagnetic coil. The inner Rogowski coil measures the plasma current being undisturbed by the current in the liner. The inner toroidal coils measure the toroidal field without the effect of the field penetrating through the liner. The most important contribution is provided by the diamagnetic coil used to establish the thermal plasma energy and the energy confinement time.

First results from testing the new system are presented in this thesis. The coils were tested and calibrated, with the offsets and parasitic artefacts removed. They now measure with enhanced precision and have been embedded into the shot web-page and database of the GOLEM tokamak together with the calculated thermal plasma energy and the energy confinement time.

Keywords: magnetic diagnostics, Rogowski coil, diamagnetic coil, thermal plasma energy, energy confinement time.

Contents

Chapter 1

Introduction

1.1 Project Environment

The GOLEM tokamak is an educational device [1, 2] which was constructed in the Kurchatov Institute of Atomic Energy in Moscow to originally study plasma interactions with waves. At that time it was called $TM1$, later called $TM-1-MH$. In 1976, it was transferred to the Institute of Plasma Physics of the Academy of Sciences of the Czech Republic and was renamed in 1977 as CASTOR (Czech Academy of Sciences TORus). Its name was changed once again in 2007 to its current name, Tokamak GOLEM when it was given to the Czech Technical University in Prague, the Faculty of Nuclear Sciences and Physical Engineering. The GOLEM tokamak is a sub-part of the the PlasmaLab@CTU.

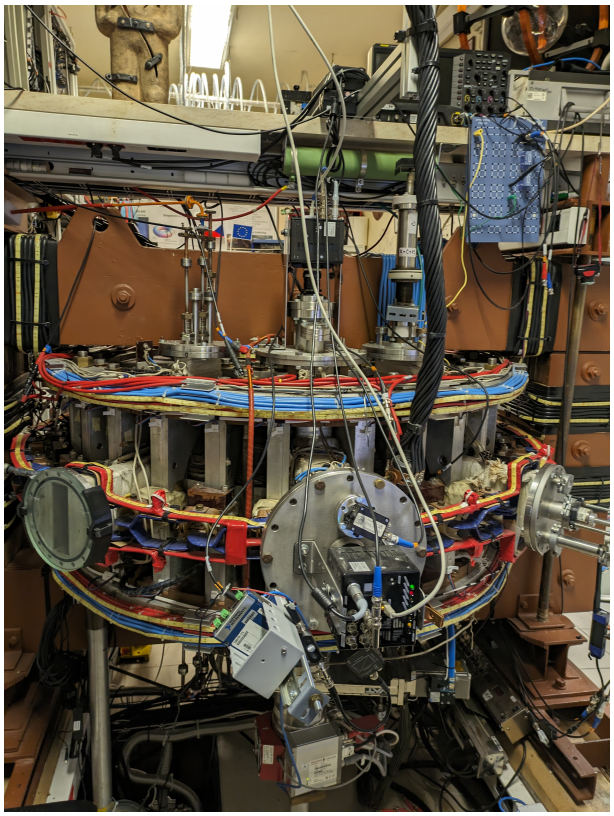

Figure 1.1: Tokamak GOLEM in its current state

Major Radius, R_0	0.40 m
Minor Radius, a	0.085 m
Electron Temperature, T_e	< 80 eV
Electron density, n_e	$3 \times 10^{18}\ m^{-3}$
Plasma Current, I_p	< 8 kA
Field Strength	0.5 T
Discharge duration	25 ms
Vessel Pressure	0.2 mPa

Table 1.1: GOLEM Parameters

1.2 Definition of Problem - Motivation

Magnetic diagnostics is one of the pillars of diagnostics and control of fusion devices. The GOLEM tokamak has implemented a standard magnetic diagnostic system [3]. For routine measurements, coils outside of the vacuum vessel are used for monitoring the toroidal magnetic field and the plasma current.

The total plasma energy and the energy confinement time are very important quantities which are not determined yet for the plasma in tokamak GOLEM. To obtain them, we need accurate measurements of plasma current and toroidal magnetic field. Putting the coils into the vacuum vessel would remove the influence of the liner and improve the reliability of the measurements.

1.3 Aim

A new system of magnetic coils placed inside the vacuum vessel of the GOLEM tokamak was designed. The system consists of one Rogowski coil (measures plasma current), two toroidal magnetic field coils situated in two locations, and two diamagnetic loops (measures toroidal flux). The aim of this thesis is to calibrate and implement the new coils and to obtain the total thermal energy of the plasma and energy confinement time.

Data derived from measurements by these coils will be analysed using related plasma physics and technology principles. In the end, results from the analysis will be presented and adapted to the GOLEM database to be available for usage in research and display for educational purposes both within the Czech Technical University in Prague and remotely.

1.4 Objectives

To achieve the aim of this work, the following will be executed:

1. the structure and state of the new inner diagnostic system will be described and discussed;
2. the magnetic coils will be tested;

3. signals from the inner Rogowski coil (for current measurement) will be analysed. The results will be compared to results from the outer Rogowski coil;
4. signals from local magnetic field measuring coils will be analysed and calibrated to determine the magnetic field strength in different locations within the tokamak;
5. signals from the diamagnetic loops will be analysed to obtain the flux changes, total plasma thermal energy and consequently the energy confinement time of the plasma.
6. the analysis and results will be adapted into the web page of GOLEM tokamak to produce automatic results for new measurements.

Chapter 2

Theoretical Framework

2.1 Nuclear Fusion Plasma

The first nuclear fusion experiment, performed in 1919 had Ernest Rutherford bombarding Nitrogen with alpha particles to form Oxygen and from which the proton was discovered [4]. The concept of mass defect was explained by Aston in 1920 [5], while Eddington suggested the conversion of Hydrogen to Helium as the source of the Sun's energy in the same year [6].The sun's energy source and processes were comprehensively explained in 1937 - 1939 by Bethe and Weizsäcker [7, 8, 9]. All events leading up to the various "Atoms for Peace" conferences resulted in a united approach in the quest to develop the best and most reliable energy source, nuclear fusion.

A fusion reaction involves two nuclei of low mass merging into a larger nucleus accompanied by the release energy. In the Sun, four protons combine to give Helium and enormous amount of energy is released. It takes about 9×10^9 years for one proton to fuse with the other in the sun's core. This reaction is possible because of the great gravitational force which keeps the particles compact for that long time that they fuse. This gravitational force overcomes the Coulomb barrier which causes a repulsion between the two positive particles

$$4p + 2e^{-} \rightarrow He + \nu_e + 26.8\ MeV. \tag{2.1}$$

Reciprocating similar reactions on earth becomes difficult as such gravitational force is not present and can not be created on earth. Yet, it is possible to achieve fusion. For instance, a deuterium and tritium nuclei can fuse to form a helium nucleus, a neutron and 17.6 MeV of energy is released:

$$D + T \rightarrow He^4 + n + 17.6\ MeV. \tag{2.2}$$

Energy released by this reaction is larger than that obtained from chemical reactions. The binding energy that holds a nucleus together is far greater than the energy that binds atoms and molecules together through chemical bonding involving electrons.This is the reason for the large release of energy. For example, the ionization energy of a hydrogen atom is 13.6 eV, being less than one millionth of the 17.6 MeV released in the D-T reaction mentioned above.

The positively charged fusing nuclei experience Coulomb repulsion. This creates a barrier which makes them difficult to fuse together. Quantum tunneling allows the particles to overcome the Coulomb repulsive barrier. Particles at the Maxwell tail (high temperature) have a higher probability of overcoming this Coulomb barrier. High temperatures up to millions of

degrees are required. For this reason, nuclear fusion is also called thermonuclear fusion.
High temperatures imply that most of the gas particles become ionized releasing free electrons. The entire ensemble of particles could be considered electrically neutral under certain conditions. This ensemble is known as plasma. Plasma is defined as a quasi-neutral gas of charged and neutral particles which exhibits collective behaviour [10].
Achieving fusion on Earth is both a physical and technological challenge. Fusion plasma as said, has to be created with reactants of sufficiently high temperature and density. This must be maintained for a sufficiently long time and the plasma restrained from any surrounding material walls. So it becomes necessary to confine the plasma in space. However, two main approaches for achieving this have been developed: magnetic confinement and inertial confinement.

1. Magnetic Confinement: This mode uses magnetic field for the confinement of plasma. Magnetic confinement fusion is currently the most promising path to developing future fusion reactors. In magnetic confinement fusion, coils are shaped to various designs to achieve confinement. The most promising and common configurations for magnetic confinement are:
    - Tokamak Configuration
    - Stellarator Configuration
2. Inertial Confinement: This is confinement involving heating achieved by compression.Inertial confinement fusion works primarily by a pulse method. In these devices, thermonuclear fusion is achieved through micro-explosions of reactant targets induced by high power laser or particle beams.

2.1.1 Plasma Properties

Plasma is considered to have a net neutral charge. This is called quasi-neutrality and for this reason, there is ideally no net electromagnetic forces on it. So in this simplest case of plasma, molecules are allowed free movement and collide with other molecules. In the real sense, within a plasma, the particles are forced to move around, and can locally concentrate positive or negative charges, generating electric fields within the plasma. Magnetic fields can also be created due to the current generated by the motion of plasma particles. The magnetic and electric fields, though local, are able to affect remote regions within the plasma. This is known as the collective behaviour of plasma.
Plasma is also known to shield electric potentials applied to it. This is a consequence of its quasi-neutrality as well as the high collision rates of plasma which reduces the ability of particles to react to fields. Quasi-neutrality is the state of the plasma when the density of ions and electrons are considered equal and a common value can be used to represent both, $n_e \simeq n_i \simeq n$.
When electric field is introduced, electrons are attracted to the positive charge in plasma, shielding the electric field from the positive charges, hence the field does not penetrate into the plasma. The ions do the opposite. This shielding effect of the external field exist over a certain distance known as the Debye length, λ_D defined as:

$$\lambda_D \equiv \sqrt{\frac{\epsilon_0 k_B T_e}{n e^2}}, \tag{2.3}$$

where ϵ_0 is the permittivity of free space, k_B is Boltzmann constant, T_e is electron temperature and n is the plasma density. This shielding effect is also valid within a conceptual volume in

the plasma known as the "Debye sphere":

$$V_D = \frac{4}{3}\pi {\lambda_D}^3, \tag{2.4}$$

with the λ_D as the radius [10]. For quasi-neutrality, the Debye length should be much smaller than the plasma dimension $\lambda_D \ll L$.
The number of particles contained in a Debye sphere is called the plasma parameter:

$$N_D = n \cdot \frac{4}{3}\pi {\lambda_D}^3. \tag{2.5}$$

For a system to be considered a plasma, the plasma parameter, N_D should be much greater than unity, $N_D \ggg 1$.
Also, ionized gases qualify to be called plasma if the oscillation frequency, ω and the mean time between collisions with neutral atoms τ combine in such a way that $\omega\tau \gg 1$.
The necessary properties of a plasma are summarised thus:

1. $N_D \gg 1$
2. $\lambda_D \ll L$
3. $\omega\tau \gg 1$

2.2 Tokamaks

Plasma is confined in order to achieve ignition ($Q = \infty$). Q-value is the ratio of the output power from fusion reactor to the power losses.The condition for ignition is characterised by the Lawson criterion (also called "triple product"), which is the product of the density (n), temperature (T) and the duration of energy confinement (τ_E) [10].

$$nT\tau_E \geq c_{crit} \tag{2.6}$$

For $D-T$ fusion,

$$c_{crit} = 5 \times 10^{21}.$$

Magnetic field confines plasma when applied in linear configuration but this is not sufficient as the plasma particles are lost largely at the edges. These end losses hinders the attainment of the desired energy confinement time. The end losses are mitigated if the linear field is rolled into a simple torus.However, a new problem arises as a toroidal magnetic will have a gradient which causes drifts of the ions and electrons in opposite directions, leading to charge separation which corresponds to electric field creation. A coupling of this generated electric field and the background magnetic field leads to an outward drift called $\vec{E} \times \vec{B}$ - drift. Particles are lost in this drift and to mitigate these losses, magnetic field lines are twisted so that accumulation of charges is compensated at each edge by a change of polarity. These twisted field lines concept is actualized in the tokamak and stellarator.
The tokamak is a ring-shaped vacuum vessel placed as the secondary circuit of a transformer. Plasma is confined inside by a strong magnetic field along the chamber and it is heated by electric current [11].
The Tokamak consists majorly of:

1. Toroidal magnetic field

2. Conducting ring
3. Vertical magnetic field (figure 2.1)

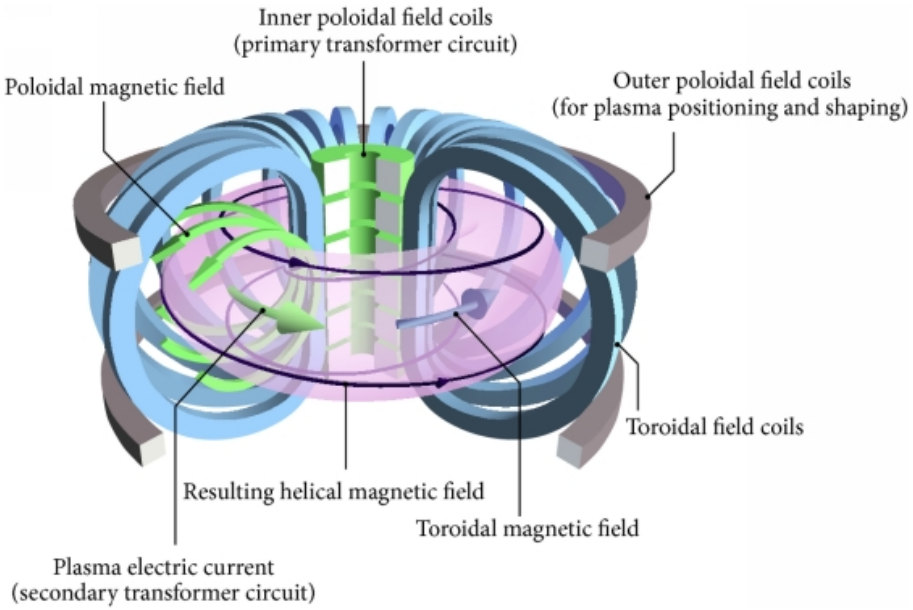

Figure 2.1: Tokamak field components [12]

The conducting ring is a current loop. In the case of the tokamak, the conducting ring is the plasma itself. Current flowing through plasma creates series of surfaces with constant flux as the same number of induced field lines crosses it. These surfaces are called toroidal flux surfaces. The problem is that these surfaces could be infinite and the shape will be too large and inappropriate to be housed by a vessel and Lorentz forces will push the plasma outwards. To obtain a more desirable shape of the flux surfaces, a vertical magnetic field is added using two coils arranged toroidally at the top and bottom. The current loop symmetry is maintained while also adding a contribution to the toroidal flux. The third phase is to add the toroidal magnetic field using coils arranged poloidally and the Tokamak is complete. The presence of the plasma as the current loop creates the required twist of the field lines. The current loop also plays a role in plasma build up and plasma heating and is produced by induction with the plasma acting as the secondary coil of transformer. This makes the Tokamak to be a none steady-state device.

2.3 Plasma Beta, β_{plasma}

One of the most important parameters of fusion devices is the plasma beta, β. Plasma beta is defined as the ratio of kinetic pressure p , to the magnetic pressure.

$$\beta_{plasma} = \frac{kinetic\ pressure}{magnetic\ pressure} = \frac{p}{B^2/2\mu_0} \tag{2.7}$$

When the magnetic field dominates in the plasma, $\beta \ll 1$, the plasma is forced to move along with the field. In the opposite case, when the field is weak, $\beta \gg 1$, the field is swirled along by the fluid and instabilities arise. The magnitude of fusion power generated

is directly proportional to the plasma pressure. The magnetic field and the size of a fusion device determines a large chunk of the cost, hence the need to maximize plasma beta for a commercial fusion power plant. The plasma beta is very important as it has implications on stability, confinement and even fusion power generated.

2.4 Tokamak Field Configuration

2.4.1 Flux Surface

The equilibrium equation, 2.12 for an axisymmetric system like the tokamak can be written as a diferential equation in the poloidal flux. This equation is referred to as the Grad-Shafranov equation.

$$R\frac{\partial}{\partial R}\frac{1}{R}\frac{\partial \Psi}{\partial R} + \frac{\partial^2 \Psi}{\partial z^2} = -2\pi\mu_0 R^2 \frac{dp}{d\Psi} - 2\pi {\mu_0}^2 f \frac{df}{d\Psi} \tag{2.8}$$

The Grad-Shafranov equation can be expressed in a concise form as:

$$\Delta^* \Psi + {\mu_0}^2 f(\Psi) f'(\Psi) + 4\pi^2 \mu_0 R^2 p'(\Psi) = 0 \tag{2.9}$$

Here, $\Delta^* = R\frac{\partial}{\partial R}\frac{1}{R}\frac{\partial}{\partial R} + \frac{\partial^2}{\partial z^2}$ is called an elliptical operator and $f(\Psi) = \frac{RB_\phi}{\mu_0}$ is the flux function which gives the poloidal flux associated with a unit toroidal angle ϕ.
The Grad-Shafranov equation can be attempted to be solved numerically and profiles of current, pressure and magnetic field could be obtained. An example is with the use of the EFIT code [13] which gives results of the flux within a desired space of any real plasma. When these fluxes are combined, we get series of surfaces which are called flux surfaces. On a flux surface, the pressure and magnetic flux and other flux functions are constant [10].

2.4.2 Tokamak Safety Factor

The safety factor is defined as the ratio of the poloidal turns around the torus to the number of times it wraps toroidally. It is also the ratio of the toroidal flux to the poloidal flux:

$$q_s = \frac{d\Phi}{d\Psi} \tag{2.10}$$

with the assumption of a tokamak with circular cross-section, both poloidal and toroidal magnetic flux can be approximated as:

$$d\Psi = 2\pi R B_\theta,$$

$$d\Phi = 2\pi r B_\phi,$$

With these expressions, the safety factor is expressed as:

$$q_s = \frac{rB_\phi}{RB_\theta}. \tag{2.11}$$

Safety factor is an important parameter in the study and operation of tokamaks. The safety factor is related to the stability and confinement properties of the plasma.

2.5 Theory of Plasma Diamagnetism

Toroidal magnetic field is necessary for plasma confinement. The behaviour of toroidal flux in the presence of plasma is important.
Plasma presence leads to a decrease of the toroidal flux within the plasma. This implies that plasma is inherently diamagnetic. Interestingly, in the case of tokamaks, plasma current, I_p is a necessary ingredient also. This current induces a magnetic field which combines with toroidal magnetic field to form helically twisted field lines which are associated with a parallel current called Pfirsch-Schlutter current. The Pfirsch-Schlutter current makes an increase in the vertical magnetic field, B_z. This increase in B_z also implies that plasma current makes plasma paramagnetic.

Summarily, there is a net flux change due to two magnetic contributions of the plasma:

- paramagnetic effect of longitudinal plasma current
- diamagnetic effect of the plasma due to ion cyclotron motion

The mathematical development for these different contributions to the flux change done in cylindrical coordinates involves combining $\vec{J} = \nabla \times \frac{\vec{B}}{\mu_0}$ with equilibrium MHD equation,

$$\nabla p = \vec{J} \times \vec{B} \tag{2.12}$$

with additional simplifications like neglecting toroidal contributions in the equation below:

$$\Delta\Phi = \int_S \Delta\vec{B} \cdot d\vec{S} = \pi\mu_0 \int_0^a r^2 \Delta J_\theta(r) dr \tag{2.13}$$

$$\Delta\Phi = \frac{\pi\mu_0}{B_0} \left\{ \int_0^a r^2 \frac{dp}{dr} dr + \int_0^a r^2 j_z B_\theta dr \right\}, \tag{2.14}$$

here a is the minor radius of the Tokamak. J_θ is gotten from the MHD equilibrium equation 2.12 as:

$$J_\theta = \frac{1}{B_0}(\frac{dp}{dr} + B_\theta j_z), \tag{2.15}$$

$$\Delta\Phi = \frac{\pi\mu_0}{B_0} \left\{ \int_0^a r^2 \frac{dp}{dr} dr + \int_0^a r^2 j_z B_\theta dr \right\}, \tag{2.16}$$

so the kinetic energy contribution is kinetic contribution (diamagnetic effect) is:

$$\frac{\pi\mu_0}{B_0} \int_0^a r^2 \frac{dp}{dr} dr = -\frac{\mu_0 W_\perp}{B_0}, \tag{2.17}$$

where $W_\perp$ is the perpendicular component of energy in the plasma, while the current contribution (paramagnetic effect) is:

$$\frac{\pi\mu_0}{B_0} \int_0^a r^2 j_z B_\theta dr = \frac{(\mu_0 I_p)^2}{8\pi B_0}. \tag{2.18}$$

Both can be combined to get the total change in flux in the plasma:

$$\Delta\Phi = \frac{(\mu_0 J_p)^2}{8\pi B_0} \left\{ 1 - \frac{8\pi}{\mu_0 {I_p}^2} W_\perp \right\}. \tag{2.19}$$

$\Delta\Phi$ is very useful for obtaining the total thermal energy of the plasma[11, 14, 15].

Chapter 3

Diagnostics in Tokamak GOLEM

3.1 GOLEM Discharge Procedure

The toroidal field $B_t$of the circuit is generated by 81 mF capacitors producing about 1300 V which is triggered using a thyristor into 28 poloidal coils. A similar circuit with 11 'mF capacitor and about 700 V discharges into the primary coil to set up the toroidal electric field which generates the plasma current, I_p. A time delay is created between the activation of both circuits by a time delay triggering system. This delay could be up to 20 ms [16]. Vessel pressure is regulated by a vacuum system or pumping while a gas handling system regulates the pressure of the working gas. An electron gun is used for pre-ionizing the working gas and in the case of GOLEM, tungsten filament is used. Further ionisation is caused by the avalanche process which involves numerous collisions between charged gas particles and neutrals. Induction of current in the plasma further heats up the plasma and increases ionisation until the discharge is terminated. GOLEM has a robust data acquisition system linked to an online diagnostic database. The device can also be operated remotely using the online operation command system [17].

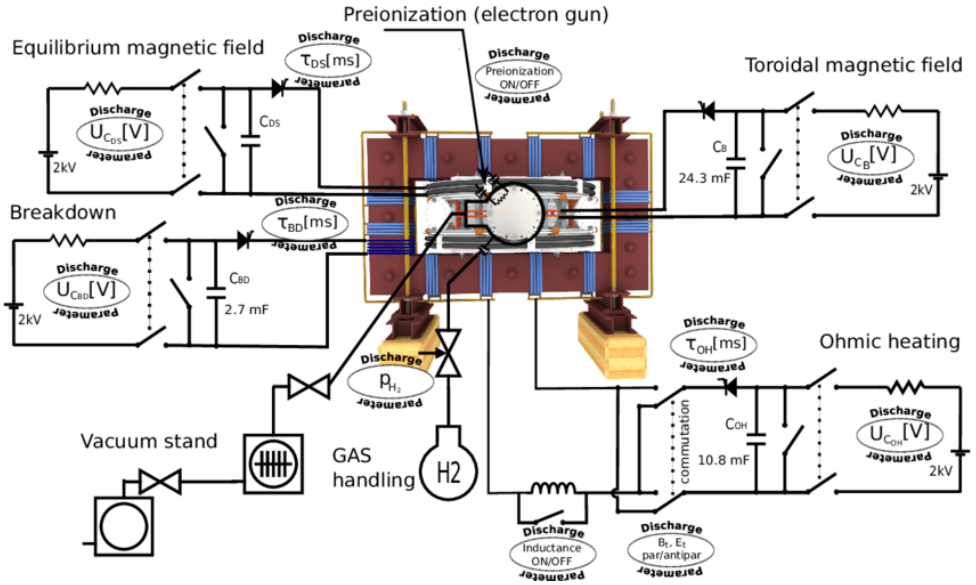

Figure 3.1: Experimental setup of Tokamak GOLEM [16]

Tokamak GOLEM still has a wide range of diagnostic tools. There are coils and loops which

take magnetic measurements, various kinds of probes as well as the presence of fast cameras from which plasma position can also be obtained.There are also hard X-ray diagnostics for runaway electron studies, bolometry, fast cameras [18] etc. The focus of this thesis are the magnetic diagnostics, so these will be described.

3.2 Basic Parameters

The basic parameters of the plasma at GOLEM are obtained with a system of diagnostics (shown in figure 3.2). The Rogowski coil is used for measuring the current flowing through the plasma. As it is wrapped around the vessel, it measures both plasma current and the current flowing through the liner. The loop measures the loop voltage, U_l corresponding to the toroidal electric field in the tokamak. The toroidal field is measured by a coil at the top high field side of the tokamak. The H_α detector gives an information about the neutral hydrogen and thus plasma confinement. Screenshots of the GOLEM shot web page with plots of basic parameters of a typical discharge with plasma as well as some other diagnostics are shown in figures 3.3, 3.4 and 3.5 .

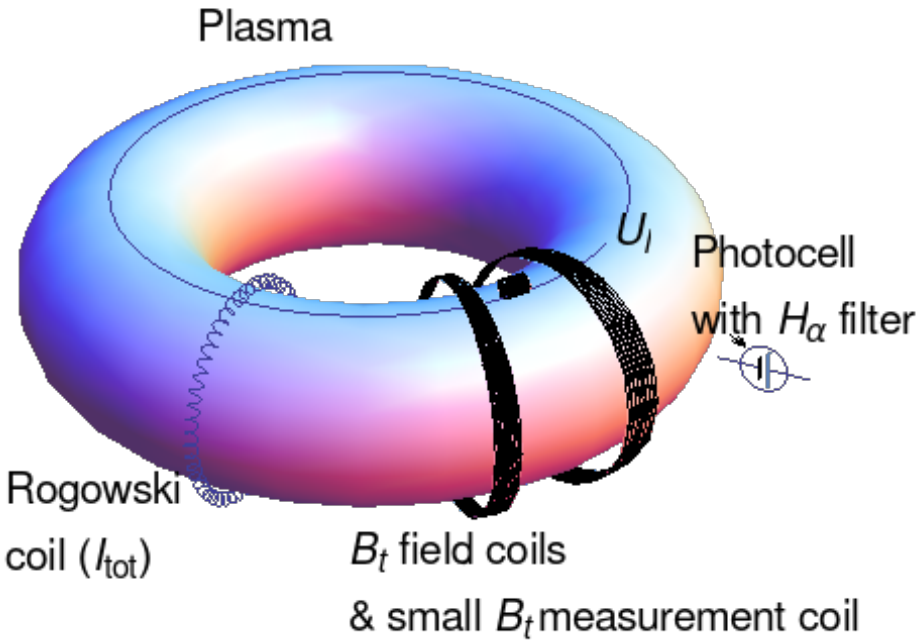

Figure 3.2: Basic diagnostic system at GOLEM

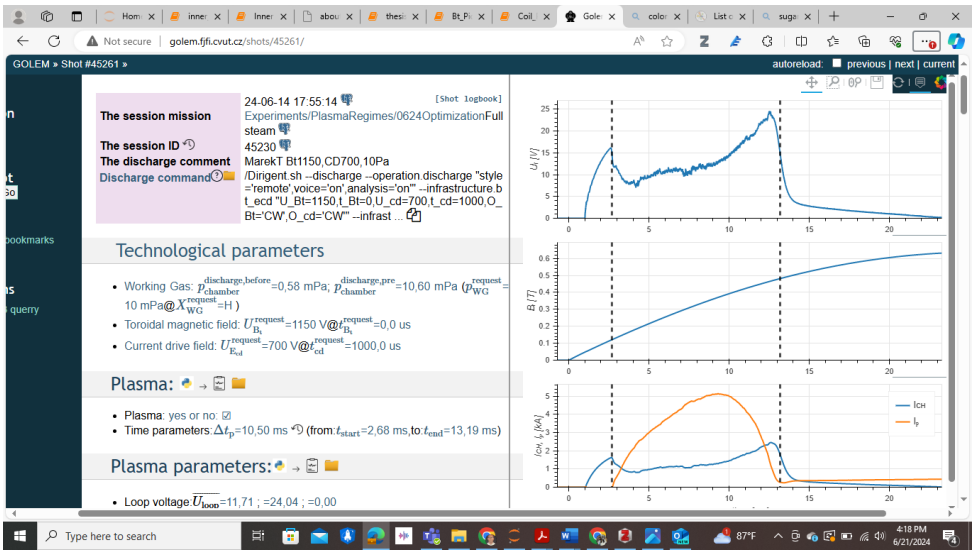

Figure 3.3: Screenshot of the GOLEM web page for a typical plasma shot with technological parameters. Plasma current I_p, loop voltage U_{loop} and toroidal magnetic field B_{tor} are shown.

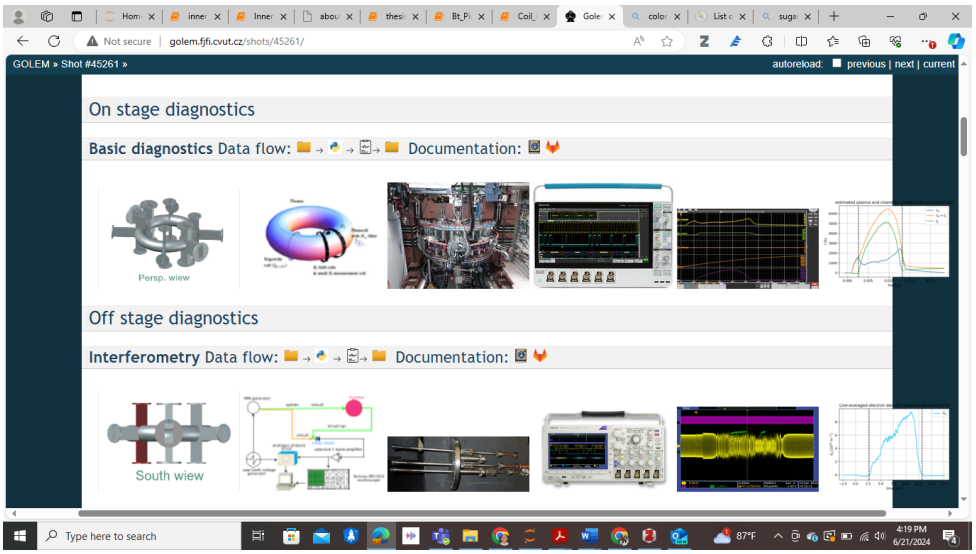

Figure 3.4: Screenshot of the GOLEM web page for a typical plasma shot showing some diagnostics.

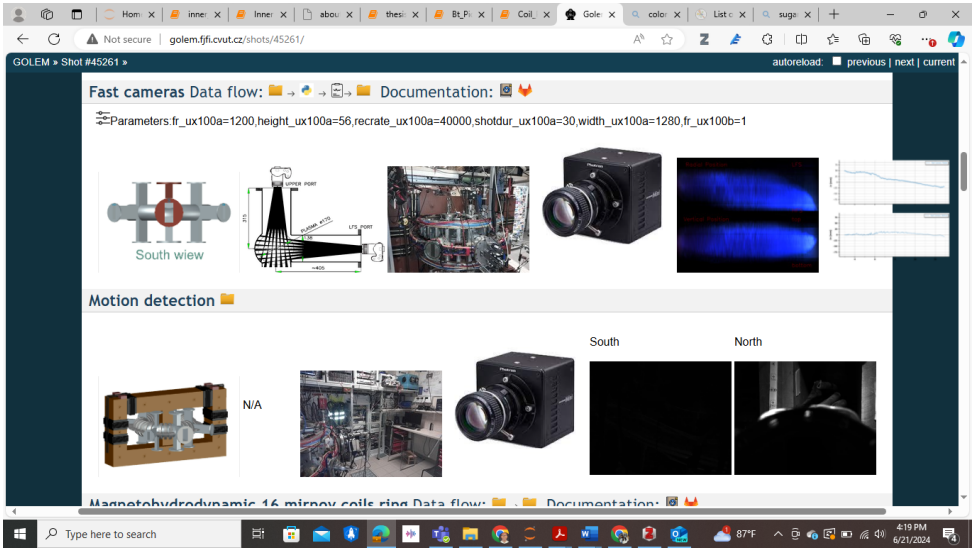

Figure 3.5: Screenshot of the GOLEM web page for a typical plasma shot showing some diagnostics.

3.3 General Principle of Magnetic Measurements

Magnetic measurements in fusion devices are made by magnetic coils which detect signals. These signals are actually the first time derivative of the magnetic field (although Hall detectors measure the magnetic field directly) as contained in Faraday's law in its integral form:

$$\oint_l \vec{E} \cdot \vec{dl} = - \oint_S \dot{\vec{B}} \cdot \vec{dS} \tag{3.1}$$

The measured signal is equivalent to the integral of the electric field over a closed loop. Hence, it is a voltage measurement.

$$\oint_l \vec{E} \cdot \vec{dl} = U_{sig} \tag{3.2}$$

3.4 Rogowski Coil

The Rogowski coil combines the Faraday's law and the Ampere's law as its principle for measurement. Faraday's law gives the relation between flux and voltage while Ampere's law relates the magnetic flux to the generating current.It is an inductive-type sensor and is known to be capable of detecting high currents [19].

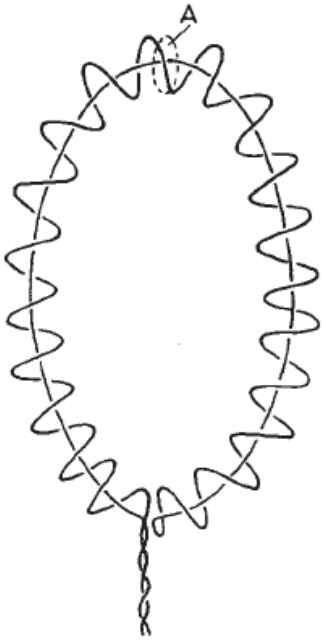

Figure 3.6: Working principle of a Rogowski coil. [20]

The total flux linkage can be determined, considering that the magnetic field induced by current enclosed by the Rogowski coil is varying little over one poloidal turn of the coil. This is a consequence of the small area turns of the Rogowski coils.

$$\phi = n \oint_l \oint_S dS \vec{B} \cdot \vec{dl}. \tag{3.3}$$

In the equation 3.3, n represents turns per unit length, S is area of each turn and l length of Rogowski coil. With Ampere's law, we have:

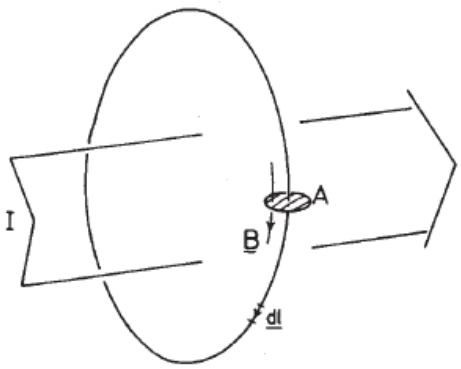

Figure 3.7: Geometry for Rogowski coil integration path [20]

$$\mu_0 I = \oint \vec{B} \cdot dl. \tag{3.4}$$

When we include Faraday's law relating measured signal with rate of flux change:

$$U_{sig} = \dot{\Phi}, \tag{3.5}$$

we get the principal Rogowski coil equation:

$$I = \frac{1}{nS\mu_0} \int_0^t U_{sig}(\tau) d\tau. \tag{3.6}$$

Rogowski coils are used to measure the current of the plasma as well as other conductors in a tokamak. In GOLEM, the Rogowski coils measurements contain both because the coil covers the chamber and the plasma.To obtain the plasma current, the conducting chamber current has to be subtracted as follows:

$$I_p(t) = I_{tot}(t) - I_{ch}(t). \tag{3.7}$$

Here, I_{tot} is the total current obtained from U_{sig} measured by the coils, while I_{ch} and I_p are the chamber and the plasma current respectively.
The chamber current is obtained by solving the initial value problem using the resistance, R_{ch} and inductance, L_{ch} of the chamber material as well as the loop voltage:

$$\frac{dI_{ch}}{dt} = \frac{1}{L_{ch}}(U_l - I_{ch}R_{ch});\ I_{ch}(0) = 0. \tag{3.8}$$

The plasma current is:

$$I_p(t) = \frac{1}{nS\mu_0} \int_0^t U_{sig}(\tau) d\tau - I_{ch}. \tag{3.9}$$

Figure 3.8: Outer Rogowski coil at GOLEM

Some advantages of the Rogowski coils are its linearity over wide frequency band and principal capability of measuring high currents[3, 21]. The technical parameters of the Rogowski coils in GOLEM are represented in table 1.1

Length [cm]	Diameter [cm]	n $[m^{-1}]$	$\frac{1}{nS\mu_0}[(AVs)^{-1}]$
230	0.8	$3 \cdot 10^3$	$5.3 \cdot 10^3$

Table 3.1: Technical parameters of the outer Rogowski coil at GOLEM[3]

3.5 Flux Loops

Poloidal magnetic flux Ψ, and toroidal magnetic flux ϕ, are important quantities in fusion. For tokamaks, flux loops are employed to obtain both toroidal and poloidal fluxes. They are made up of single turns and they detect average magnetic flux across the effective area of the loop. Similarly, this measurement procedure involves integrating the loop voltage, U_{loop} which is the original signal detected by the loops as contained in Faraday's law and can physically be understood as the line-integrated intensity of toroidal electric field [3]:

$$U_{loop} = \oint_l \vec{E} \cdot \vec{dl} = 2\pi R E_\phi \tag{3.10}$$

The flux is represented thus:

$$\Phi(t) = \int_{S_l} \vec{B} \cdot \vec{dS} = \int_0^t U_{loop}(\tau) d\tau \tag{3.11}$$

Additional uses of the U_{loop} in GOLEM are to determine chamber current, I_{ch} which is subtracted as explained in the previous section to get the plasma current; while also being used to calculate the total ohmic heating power by current drive, P_Ω.

Flux type	N_{turn}	r $[m]$
ϕ	1	0.145

Table 3.2: Technical parameters of of the toroidal magnetic flux coil

Flux type	N_{turn}	r $[m]$
Ψ	1	0.57

Table 3.3: Technical parameters of the poloidal magnetic flux coil

3.6 Magnetic Field Measuring Coils

3.6.1 B_ϕ measuring coils

B_ϕ (toroidal magnetic field) can be obtained in various ways. One way is by using the voltage, U detected at the ends of the toroidal flux ϕ loop:

$$B_\phi = \frac{1}{A_{eff}} \int_0^t U_{sig}(\tau) d\tau \tag{3.12}$$

Here, A_{eff} is not the effective area derived from the geometry of the coil but the effective area obtained by calibration. such that the B_ϕ of the coil corresponds to that at the center of the tokamak, $B_{\phi 0}$ [3] which can be obtained analytically using the current in Ampere's law:

$$B_\phi(R) = N_c N_t \frac{\mu_0 I_c}{2\pi R} \tag{3.13}$$

N_c is the number of coils, which for GOLEM is 28 and N_t is the number of turns of each coil with I_c as the current in each turn and $R \in (R_0 - R_c, R_0 + R_c)$.

Figure 3.9: Toroidal field measuring coil at GOLEM

$D[cm]$	N	$S[cm^2]$	A_{eff} $[cm^2]$
1	255	64	147

Table 3.4: Geometrical parameters of the old B_ϕ detection coil at GOLEM

3.6.2 B_θ measuring coils

To detect B_θ, Mirnov coils uniformly distributed across the poloidal cross-section of the tokamak are employed. All the 4 coils for this purpose are located on a single circular rack inside of the liner (figure 3.10). The rack has a diameter of 9.3 cm and locations of respective coils are shown in figure (3.10). From the figure, it is possible to evaluate plasma column displacement by taking the difference of the magnitude of B_θ on opposite coils.

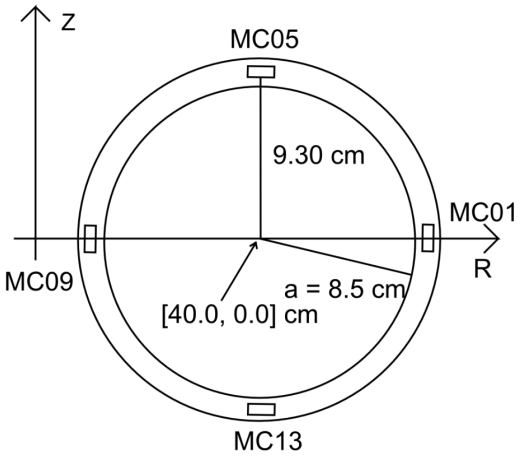

Figure 3.10: Scheme of names and spatial distribution of old Mirnov coils of tokamak GOLEM

The effective area of these coils are obtained by considering both inner and outer diameters of the coils as follows:

$$A_{eff} = N\pi(\frac{d_1 + d_2}{4})^2 \tag{3.14}$$

Due to a misalignment of three out of the four coils, they pick up signal from the toroidal magnetic field [3]. This cross-talk signal must be subtracted properly. This is done by weighting the cross-talk signal with the correct toroidal magnetic field signal obtained by the toroidal field measuring coils to get a weighting coefficient.

$r[cm]$	$l[cm]$	$d_1[cm]$	N_1	d_2	N_2	$d_{wire}[mm]$
9.3	3	0.64	46	0.66	45	0.3

Table 3.5: Technical parameters of B_θ detection coil

$L[\mu H]$	$R[\Omega]$	A_{eff} $[cm^2]$
14	1.06	37

Table 3.6: Operational parameters of B_θ detection coils

Other magnetic coils are the stabilization coils used for plasma positioning and the 16 MHD coils inside the liner which are used for detecting MHD activity.

Chapter 4

The New Inner Magnetic Diagnostics System

4.1 Rogowski Coil

The new Rogowski coil installed inside of the chamber is designed to measure the plasma current, I_p directly without the influence of the current in the liner as is in the case of the outer Rogowski coil. It is mounted in a mechanical support. This support structure also holds the other internal diagnostic coils.

The coil is made of enamelled Copper wire of diameter, $0.3mm$ and insulated from short circuiting with teflon tape.. The wire of length, 125.66 cm is wound 1974 times into small torus of 1 cm diameter uniformly (figure 4.1). The parameters of the inner Rogowski coil are

Figure 4.1: New Inner Rogowski Coil Insulated with Teflon Tape.

shown in the table 4.1.

$D\ [cm]$	$l\ [cm]$	N	$n\ [m^{-}1]$	$d_{wire}\ [mm]$	$L\ [mH]$	$R\ [\Omega]$
1	125.66	1974	1571	0.3	0.4422	13.15

Table 4.1: Inner Rogowski Coil Parameters. D is the diameter of the coil, N is the number of small turns, n is the turn density, d_{wire} is the wire diameter, while L and R and the inductance and resistance of the coil, respectively.

From the Rogowski equation 3.6, the current is obtained by integrating:

$$\dot{I} = 3.225 \times 10^6 \times U_{sig} \tag{4.1}$$

Although this new Rogowski coil should detect signals unique to the induced voltage by the current, we would later observe that there is a pick up of toroidal magnetic field at the ends of the toroidal turns. Details of how this is dealt with is discussed in the next chapter. Nevertheless, the sensitivity of the coil could still be discussed. Rogowski coil sensitivity, s is considered to be the ratio of the voltage output of the coil to the time rate of the change of current flowing through the coil [22].

$$s = \frac{U_{sig}}{\dot{I}} = \frac{\mu_0 \cdot N \cdot r^2}{2R} \tag{4.2}$$

$$s = \frac{1}{3.225 \times 10^6} = 3.10 \times 10^{-7}\ V \cdot s/A \tag{4.3}$$

By considering the estimated uncertainties in the parameters of the coil, the uncertainty of the sensitivity is obtained thus:

$$(\frac{\delta s}{s})^2 = (\frac{\delta N}{N})^2 + (\frac{\delta R}{R})^2 + 4(\frac{\delta r}{r})^2 \tag{4.4}$$

With $\frac{\delta N}{N} = 0.05$, $\frac{\delta R}{R} = 0.1$ and $\frac{\delta r}{r} = 0.05$, the uncertainty, $\delta s = 0.46 \times 10^{-7}$.

$$s = (3.10 \pm 0.46) \times 10^{-7}\ V \cdot s/A \tag{4.5}$$

4.2 Local Toroidal Field Measuring Coils

Two coils have been installed to measure the toroidal magnetic field at two different locations within the Tokamak. One is located on the high field side (TF-HFS) and another on the low field side (TF-LFS).
The coils are made by wounding enamelled copper wire of diameter 0.3 mm on a teflon core of diameter, 8.6 mm and length 14 mm as shown in figure 4.2. The wire is wound 114 times around the core for the TF-HFS coil and 106 times for the TF-LFS coil. The technical parameters of both coils are summarised in tables 4.2 and 4.3.

The coils detects induced voltage and by Faraday's electromagnetic induction principle, the required measurement can be expressed in terms of the measured signal as:

$$\dot{B_\phi} = \frac{1}{A_{eff}} U_{sig}. \tag{4.6}$$

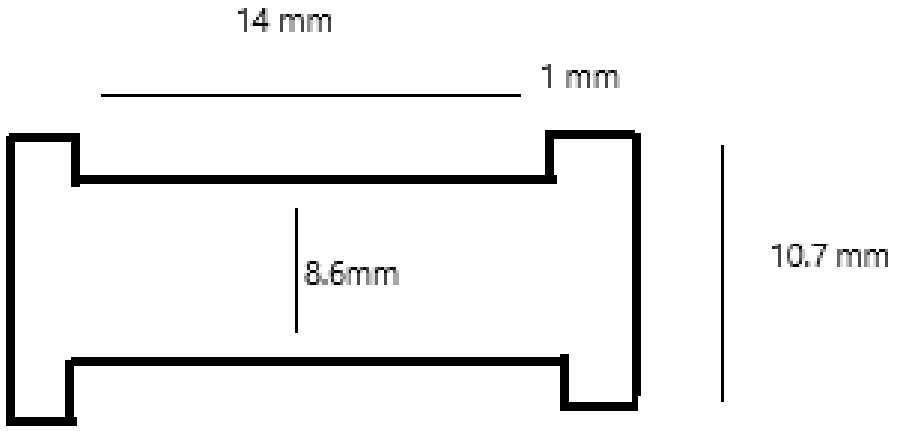

Figure 4.2: Schematics of the toroidal magnetic field measuring coil

$D\ [cm]$	$A_{eff}\ [cm^2]$	N	$d_{wire}\ [mm]$	$L\ [mH]$	$R\ [\Omega]$
0.98	172	114	0.3	0.2605	2.182

Table 4.2: High field Side toroidal magnetic field measuring coil parameters

$D\ [cm]$	$A_{eff}\ [cm^2]$	N	$d_{wire}\ [mm]$	$L\ [mH]$	$R\ [\Omega]$
0.98	159.2	106	0.3	0.2232	1.866

Table 4.3: Low field side toroidal magnetic field measuring coil parameters

The HFS and LFS expressions are:

$$\dot{B}_{\phi_{HFS}} = \frac{1}{172 \cdot 10^{-4}} \times U_{sig}, \tag{4.7}$$

$$\dot{B}_{\phi_{LFS}} = \frac{1}{159.2 \cdot 10^{-4}} \times U_{sig}. \tag{4.8}$$

4.3 Diamagnetic Loops

The diamagnetic loop is designed to measure total change of the plasma magnetic flux. So, in order to obtain the correct data, the system designed coil must enclose completely the plasma contour [20].
Figure 4.3 shows main dimensions of the diagnostic. The diagnostic consist of two concentric loops with the diameter difference large enough to detect spatial magnetic flux changes in the plasma. The diameter of the inner loop is 175 mm while that of the outer is 204 mm, with the Rogowski and toroidal field coils sited in their respective locations between both diamagnetic

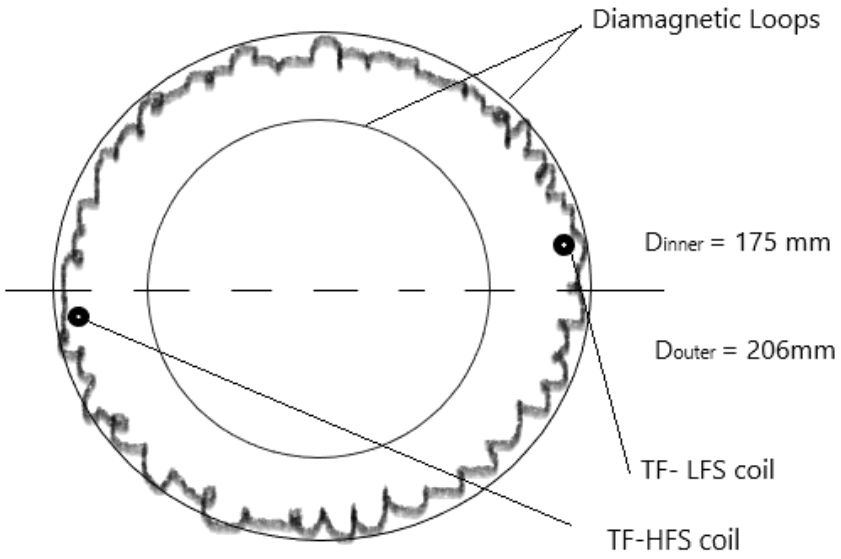

Figure 4.3: Scheme of the poloidal cross-section of the new ring.

$D\ [cm]$	$A_{eff}\ [cm^2]$	$d_{wire}\ [mm]$	$L\ [mH]$	$R\ [\Omega]$
17.50	240.5	0.3	0.005	1.170

Table 4.4: Inner Diamagnetic Loop Parameters

$D\ [cm]$	$A_{eff}\ [cm^2]$	$d_{wire}\ [mm]$	$L\ [mH]$	$R\ [\Omega]$
20.40	326.9	0.3	0.005	1.090

Table 4.5: Outer Diamagnetic Loop Parameters

loops (figure 4.3). The technical parameters of both loops are in the tables 4.4 and 4.5. The flux linking both loops are obtained by integrating the detected signal:

$$\dot{\Phi}(t) = U_{sig}. \tag{4.9}$$

The complete image of the inner magnetic diagnostic system mounted on a mechanical system is shown on Figure 4.4. Figure 4.5 shows the diagnostic system seated inside the liner.

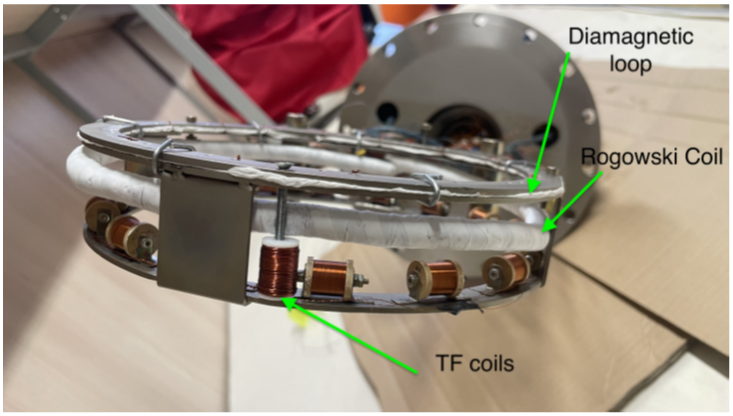

Figure 4.4: New inner diagnostics outside before installation.

Figure 4.5: New inner diagnostics installed in the tokamak.

Data from these diagnostics described are acquired using oscilloscopes with a $1\ \mu s$ time difference between each data point.

Chapter 5

Analysis of Rogowski Coil Signal

In the analysis of the signals from the Rogowski coil, shots from three experimental campaigns at GOLEM are utilized. For every campaign, new findings influence the mode of analysis employed in the next campaign. The discussion will be based on the campaigns and comparisons will be made with the old Rogowski coil measurements as well. For shots with plasma, the plasma duration is marked by dashed lines.

5.1 First Analysis - Initial Problems

Figures 5.1 and 5.2 show the raw signals of the initial shots used for the analysis. The voltage signal shows that the coil has a responsive behaviour to the presence of plasma. These signals are integrated to obtain the plasma current.

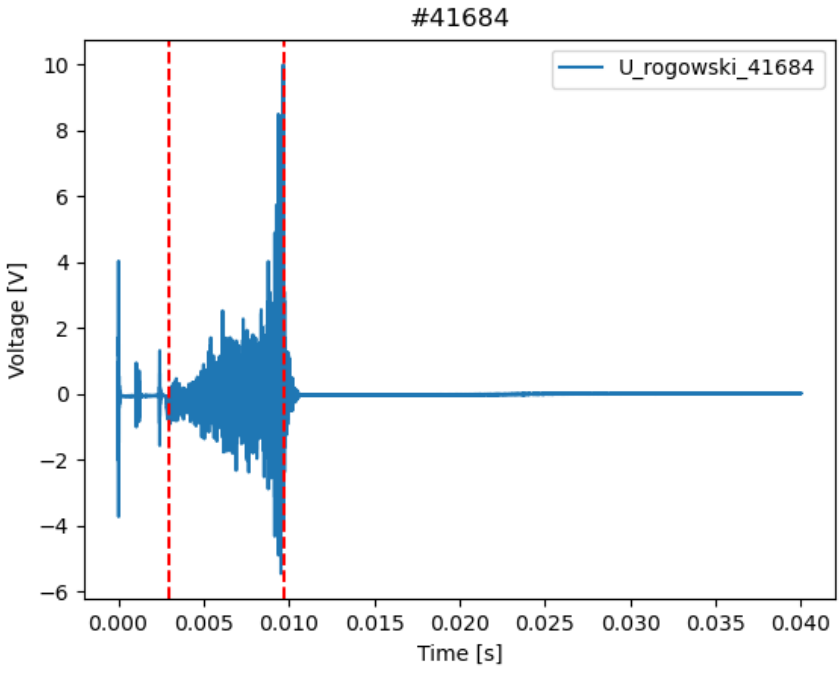

Figure 5.1: First raw signals from the inner Rogowski coil

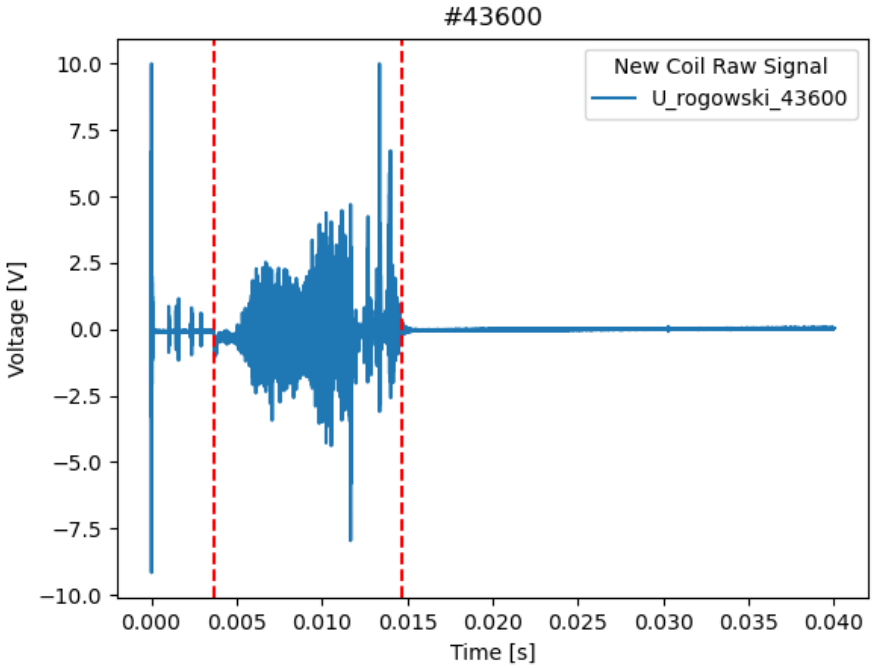

Figure 5.2: Signals from inner Rogowski coil

A direct integration of these signals using 4.1 show a large discrepancy when compared with the Plasma current measured by the Rogowski coil used in the standard basic diagnostics at GOLEM. This discrepancy is shown in figures 5.3 and 5.4.
Firstly, one of the problems of the outer Rogowski coil is observed. The plasma current does not terminate even when the plasma duration ends. With this observation, it becomes necessary to also probe the method by which the plasma current is obtained from the outer Rogowski coil measurement. It is suspected that the modelling of the current in the chamber, I_{ch} has some offset and has to be remodelled. This remodelling is executed in section 5.4.

Secondly, the maximum plasma current, $I_{p_{max}}$ from the inner Rogowski coil is not the same as that of the outer Rogowski coil. For example, in figure 5.3, the outer Rogowski coil measures $I_{p_{max}} \approx 1.5$ kA while the inner Rogowski coil measures $I_{p_{max}} \approx 3.0$ kA (about twice higher). Also, since the coil is inside the chamber, it should measure the plasma current directly and should also terminate to zero when the plasma duration ends. This is not the case, as there is a tail current persisting until the end of the shot processing.

There are two likely causes of the persistent current the higher maximum plasma current. One is the suspected cross-talk of toroidal magnetic field on the Rogowski coil signal. Another is offset created by the integration. These observed discrepancies are addressed in subsequent sections and the cause is determined simultaneously. In essence, a corrective approach was applied to determine the cause of the problem.

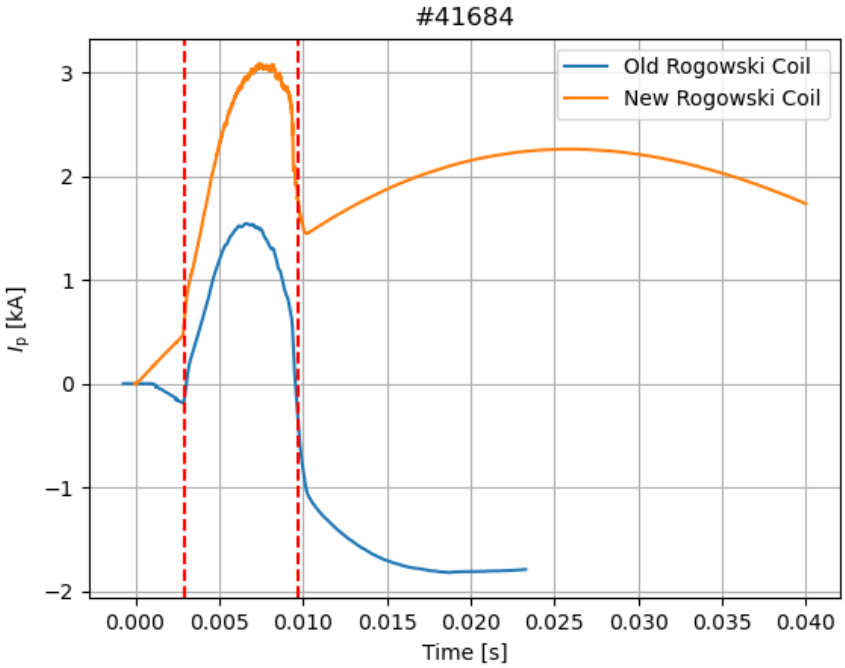

Figure 5.3: Integrated signal from the new inner Rogowski coil (blue) compared with the integrated signal from the old outer Rogowski coil (orange)

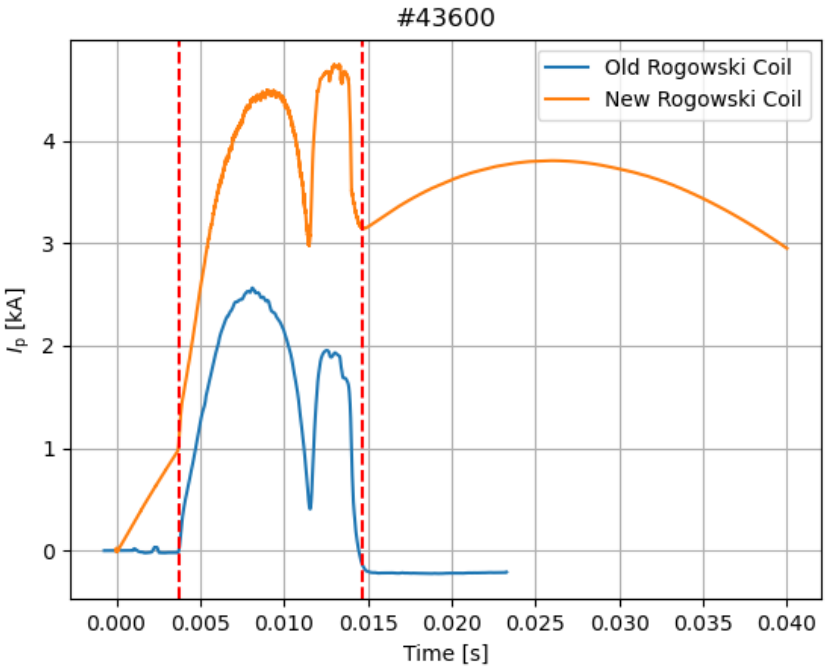

Figure 5.4: Integrated signal from the new inner Rogowski coil (blue) compared with the integrated signal from the old outer Rogowski coil (orange)

5.2 Integration Offset Removal

An attempt was made to model the offset. Some part of the raw signals (2ms before plasma and 20ms after plasma) in figures 5.1 and 5.2 were fitted to standard linear, quadratic and cubic functions. This would represent the function for the offset which is then subtracted from the raw signal itself before it is integrated. Figures 5.5 and 5.6 show the results from this operation.
After the offset removal, a better agreement is observed between the inner Rogowski coil measurement and the outer one. The maximum plasma current measured by both diagnostic are now comparable in magnitude. The quadratic fit appear to perform better than the linear and cubic fits. Yet, there is an obvious inaccuracy with the plasma duration. All three fits do not terminate convincingly with the plasma. Hence, this fitting method is not a sufficient solution to the discrepancies. As well, the presence of the integration offset is not responsible for the discrepancies either.

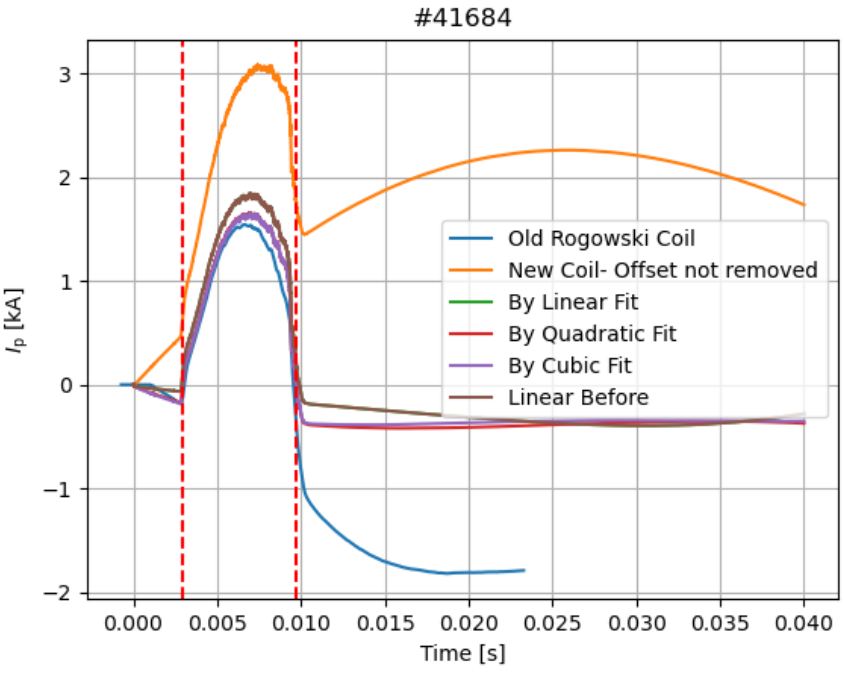

Figure 5.5: Offset fitted to different functions. Inaccuracy with plasma duration.

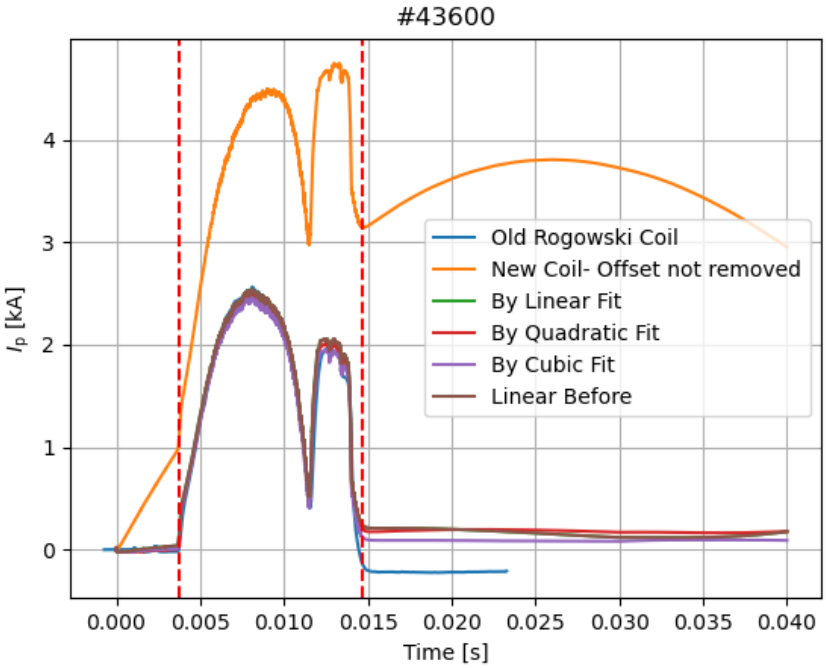

Figure 5.6: Offset fitted to different functions. Inaccuracy with plasma duration.

5.3 Toroidal Magnetic Field Cross-Talk

It is necessary to check for pick-up of toroidal magnetic field by the inner Rogowski coil, since there are inconsistencies resulting from the removal of offsets.
A new set of shots consisting of vacuum discharges and plasma discharges are executed for this investigation. The vacuum shots will show what signals the diagnostic measures in the absence of plasma. From these, there can be a comparison with the toroidal magnetic field. Ideally, the inner Rogowski coil should measure no current during a vacuum shot. Figure 5.7 shows that even for a vacuum shot, the inner Rogowski coil measures signals which have very similar shape as the toroidal magnetic field.

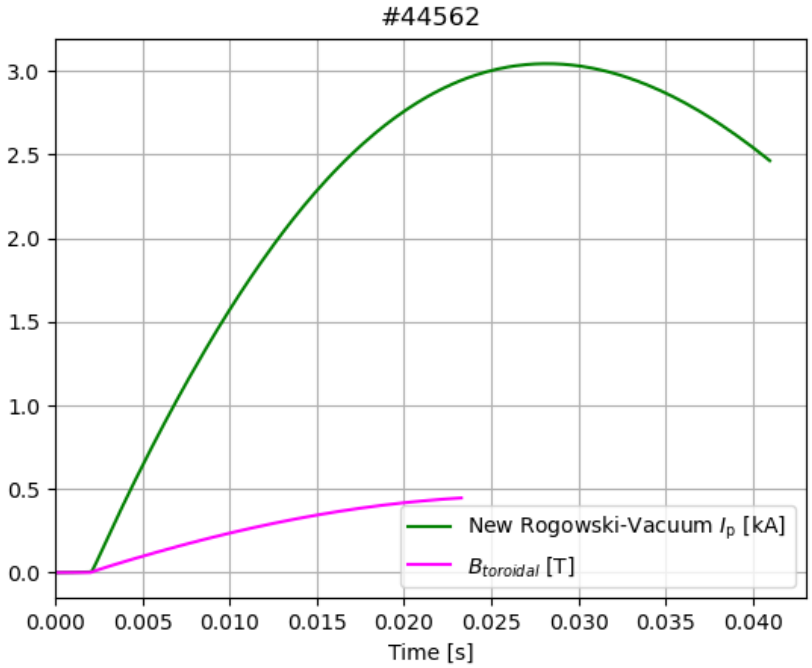

Figure 5.7: Vacuum shot comparison: Inner Rogowski coil vs toroidal magnetic field measurement - similar curve shape is observed for both.

Two methods are used for the toroidal magnetic field cross-talk removal for plasma shots. The naive method is to fit the pre-plasma and post-plasma portions of the current to the quadratic function. The second method which comes out as the better method is to fit the the pre-plasma and post-plasma portions to the function of an RLC-circuit as described in [11]. The toroidal magnetic field by induction is:

$$B_{tor} = \frac{\mu_0 N I}{2\pi r}, \tag{5.1}$$

where I is the current through the oscillating RLC circuit:

$$I = C U_0 \frac{\beta^2 + {\omega_0}^2}{\omega_0} e^{-\beta t} sin(\omega_0 t) \tag{5.2}$$

where $\beta = \frac{1}{2}\frac{R}{L}$ and $\omega_0 = \sqrt{\frac{1}{LC} - \frac{1}{4}\frac{R^2}{L^2}}$.

Equation 5.2 is parameterized as:

$$I_{Bt-cross-talk} = \alpha_1 e^{-\alpha_2 t} sin(\alpha_3 t), \tag{5.3}$$

with;

$$\alpha_1 = C U_0 \frac{\beta^2 + {\omega_0}^2}{\omega_0}, \tag{5.4}$$

$$\alpha_2 = \beta, \tag{5.5}$$

$$\alpha_3 = \omega_0. \tag{5.6}$$

Equation 5.3 is the function used for the fit and the result of this fit is shown in figure 5.8. This fit represents the cross-talk of the toroidal magnetic field on the inner Rogowski coil. The

desired constants for shot 45025 are as follows: $\alpha_1 = 4644.08$, $\alpha_2 = 13.03$ and $\alpha_3 = 50.48$. Hence, the equation:

$$I_{Bt-cross-talk} = 4644.08e^{-13.03t} \sin(50.48t). \tag{5.7}$$

Subtracting this cross-talk should give an accurate measurement of the Plasma current:

$$I_p = I_{plasma+cross-talk} - I_{Bt-cross-talk}. \tag{5.8}$$

The result of this process for a plasma shot is in figure 5.9.

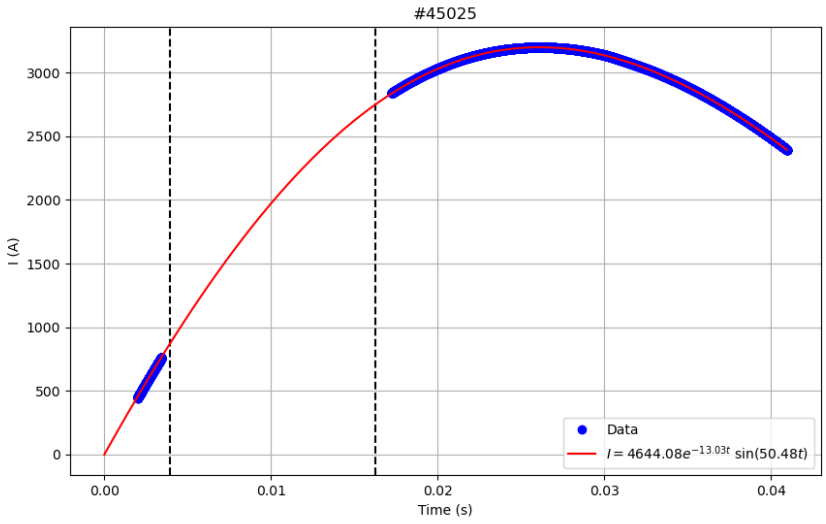

Figure 5.8: RLC Fit Performed on the Pre-plasma and Post-plasma Data of the Rogowski Coil Measurement. The Function Describes the Data Accurately.

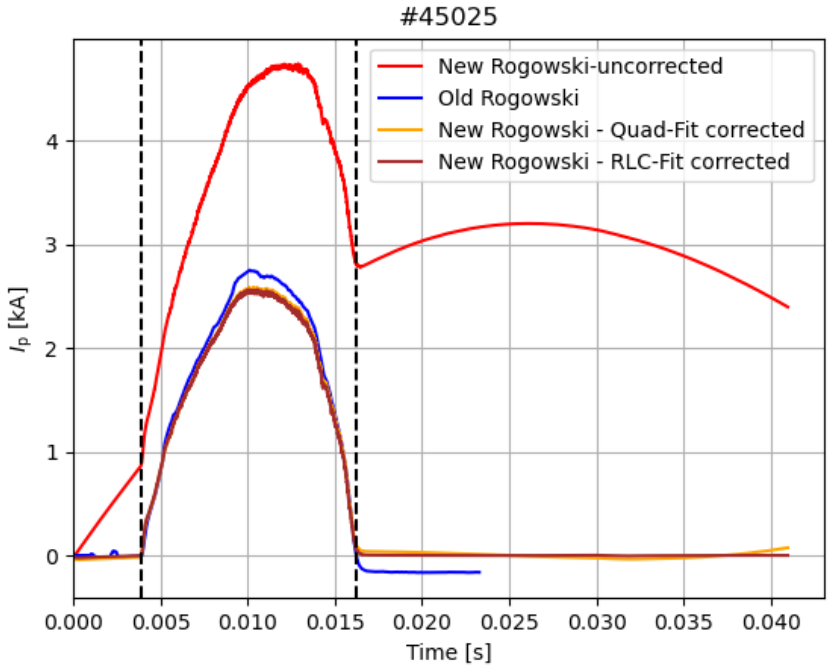

Figure 5.9: Plasma current measurement: RLC-fit vs quadratic fit. The RLC-fit method gives a very accurate result.

The plasma current measurement is the best when the RLC-Fit for the toroidal magnetic field cross-talk is used. Figure 5.9 shows $I_p = 0$ before and after plasma duration, indicating that this fit models the toroidal field cross-talk in the best way. The accuracy of the RLC modelling also confirms that the initial discrepancy discussed in section 5.1 is caused by the toroidal field cross-talk for the Rogowski coil.

Shot Number	UB_t [V]	α_1	α_2	α_3
45085	400	2991.88	16.67	46.97
45086	400	2634.39	14.23	48.91
45081	600	4257.44	16.72	47.24
45089	600	3896.38	15.88	47.43
45023	800	4382.02	12.34	51.53
45026	800	4545.00	12.97	50.51
45029	800	4496.02	12.92	50.52
45030	800	4540.39	13.03	50.42
45050	1000	5697.96	13.75	50.05
45083	1000	5613.12	13.28	50.37

Table 5.1: Parameters obtained from the RLC fit on the B_{tor} cross-talk for Rogowski measurement for different shots with different UB_t input.

This process was repeated for some other plasma shots with different UB_t and the different parameters are in 5.1.
From figure 5.9, the inner Rogowski coil measures a peak current lower than that of the outer Rogowski coil. The correctness of this measurement is reinforced by the fact that the plasma current of the outer Rogowski coil pushes below zero. Recall that this current is obtained by subtracting the chamber current from the measured signal of the outer Rogowski. With this, it is important to probe the correctness of the chamber current. This is discussed in the next section.

5.4 Chamber Current Modelling

The process of plasma current measurement by the outer Rogowski was described. It involved subtracting the chamber current, I_{ch} from the total current measured. The chamber current is obtained by solving equation 3.8 using $R_{ch} = 0.0097\ \Omega$ and $L_{ch} = 1\ \mu H$. But recent observations have suggested a need for another means of obtaining the current flowing through the chamber.
The chamber current can be obtained using both Rogowski coils situated outside and inside the chamber. Subtracting the inner current measured by the inner Rogowski coil from that of the outer should give the chamber current:

$$I_{ch} = I_{outer} - I_{inner}. \tag{5.9}$$

Figure 5.10 shows the initial results. There is a difference in the new I_{ch} result. It appears to be higher than what is obtained using equation 3.8. Also, there is a mismatch between the post-plasma portion of the outer Rogowski current measurement and the old I_{ch}.

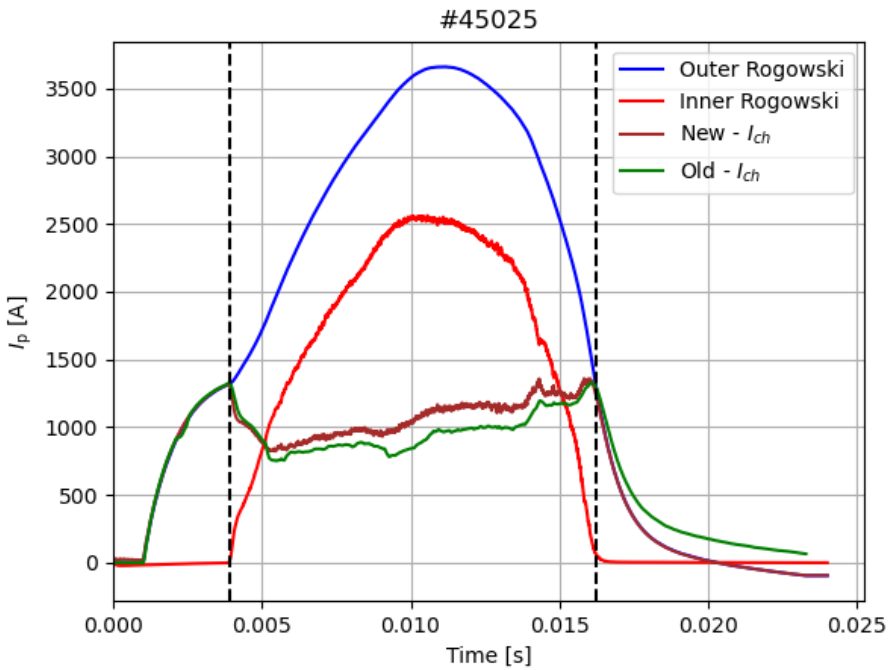

Figure 5.10: Chamber current: new vs old. New I_{ch} obtained by subtracting inner current from outer current.

This mismatch further supports the claim of inaccuracy in the chamber current measured by the outer diagnostics. There is a better match between the outer Rogowski measurement and the new I_{ch}. Yet, both do not terminate to zero at the end of the discharge but persists below to negative current values.
The probable cause of this persistent behaviour is the presence cross-talk of toroidal magnetic field in the outer Rogowski coil signal, just as observed in the inner Rogowski coil. To confirm and possibly account for this cross-talk, a series of special vacuum shots are executed. These shots are done without any current drive or gas, but with only toroidal magnetic field. For this analysis, we use the shot with $UBt = 800V$ as this is the input voltage used for the entire analysis in this work. Figure 5.11 shows the negative current produced by back induction

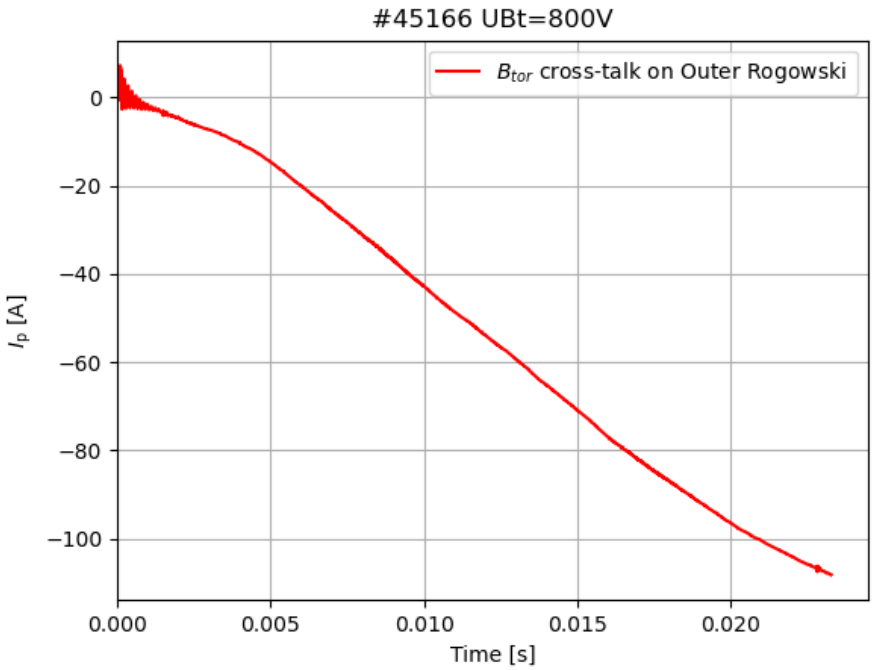

Figure 5.11: Cross-talk of B_{tor} on the outer Rogowski coil. Negative current by back induction.

of the toroidal magnetic field. When this current is subtracted from the outer Rogowski coil measurement for plasma shots, the true current from the plasma and the chamber are obtained:

$$I_{p+ch} = I_{p+ch+Bt} - I_{Bt}. \tag{5.10}$$

Consequently, when the plasma current from the inner Rogowski coil is subtracted from I_{p+Ch}, a more accurate result for the chamber current is expected:

$$I_{ch} = I_{p+ch} - I_p. \tag{5.11}$$

This complete system is shown in figure 5.12 and figure 5.13 shows the chamber current. A difference between the newly modelled chamber current (cyan) and the older (green) can be observed. This difference explains and accounts for the different I_p peaks observed in figure 5.9 and discussed in section 5.3. These findings further support the new chamber current modelling and the inner Rogowski coil measurements.
Finally, the initial value problem 3.8 is solved analytically and the newly obtained chamber current is fitted to the solution. With this fit, the resistance and the inductance of the

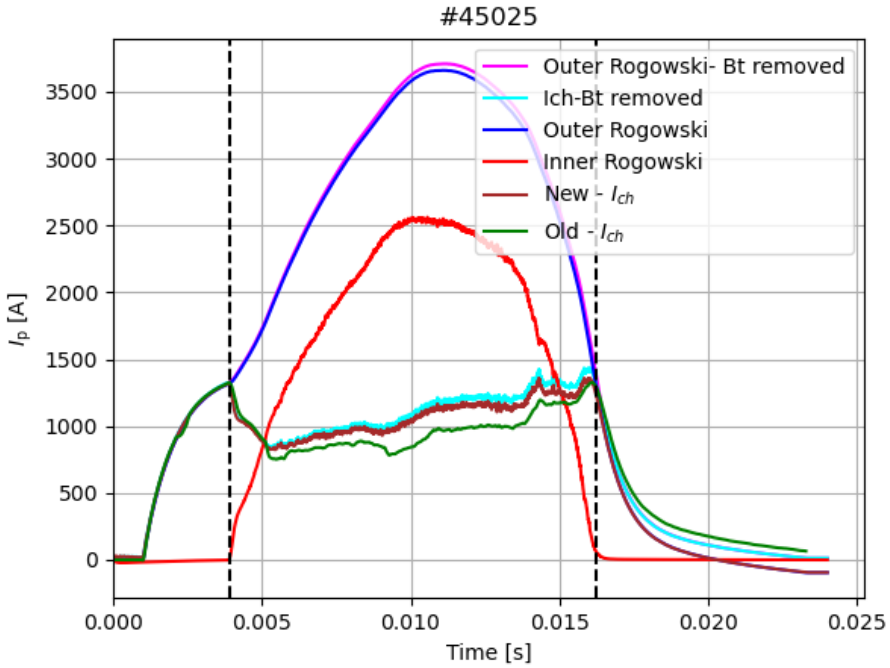

Figure 5.12: All current measurements Showing the computation of a more accurate I_{ch}. $I_{ch} - B_t$ is the resulting I_{ch} after the toroidal field pickup is removed from the outer Rogowski measurement.

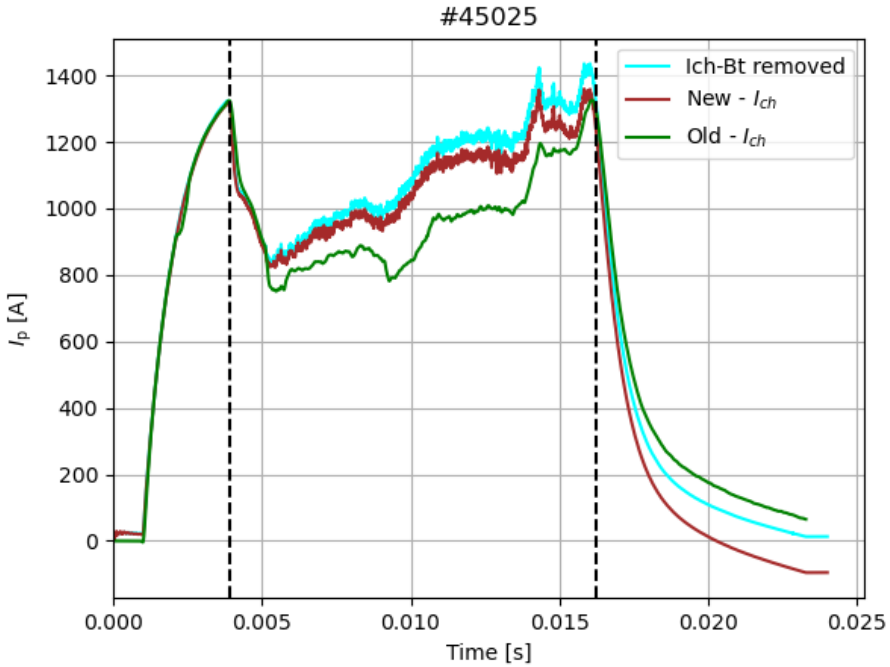

Figure 5.13: Chamber current modelling: After B_{tor} cross-talk removal, I_{ch} is more accurate and decays exponentially to zero.

chamber is obtained. The solution to 3.8 is:

$$I_{ch} = \frac{U_L}{R_{ch}} - \frac{U_L}{R_{ch}} e^{-\frac{R_{ch}}{L_{ch}} t} \tag{5.12}$$

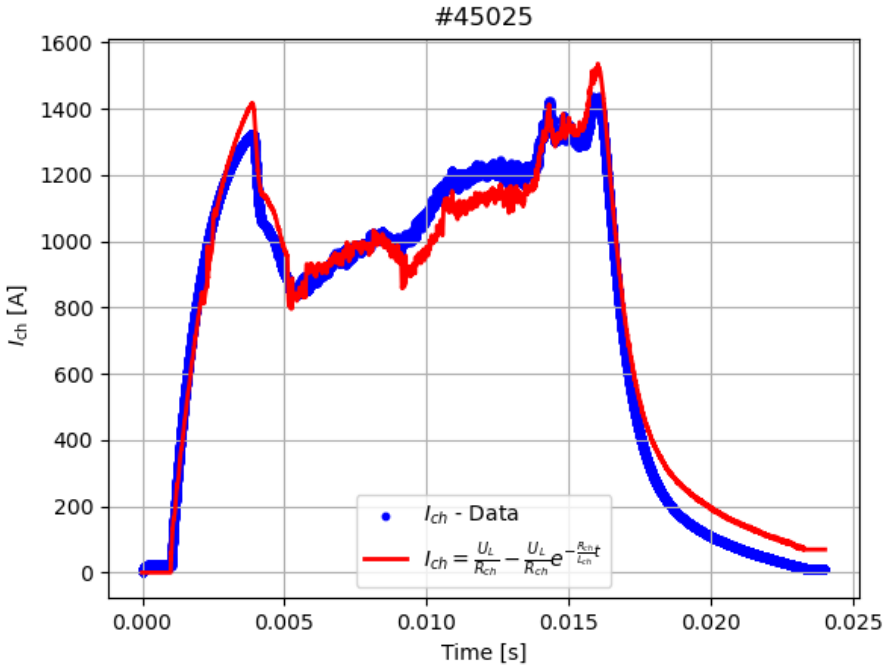

Figure 5.14: Chamber Current Modelling:Result of the fit of I_{ch} from which the resistance and inductance of the chamber is obtained.

The result of this fit is shown on figure 5.14. From the fit, the results and errors (obtained as standard deviation of the parameters) are:

$$R_{ch} = 0.00851 \pm 4.96522 \times 10^{-6}\ \Omega \tag{5.13}$$

$$L_{ch} = 1.2032 \times 10^{-5}\ \pm\ 5.0880 \times 10^{-8}\ H \tag{5.14}$$

Chapter 6

Local Toroidal Magnetic Field Measuring Coils

Shots from three experimental campaigns at GOLEM are analyzed. For every campaign, the findings remain very similar.For this reason, only one campaign is presented and shown in this analysis. Discussions cover processing of the signals from both coils located on the low field side (LFS) and high field side (HFS). The toroidal magnetic field was modelled as an RLC system as done in [11] and compared to measurements from the outer toroidal field measuring coil. Finally, the toroidal magnetic field from the local coils are used to map the the axis of the Tokamak. For shots with plasma discharge, the plasma duration is marked by dashed lines.

6.1 Raw Signals

The raw signal as described in chapter 4, is recorded as a voltage. These signals measured by the local toroidal field coils for a vacuum shot and plasma shot are shown in figures 6.1 and 6.2 respectively.
There are some important observations when comparing signals for the HFS and LFS coils for both vacuum and plasma shots:

- A sudden drop in the signal occurs for both HFS and LFS coils immediately after the capacitors are discharged (within 1 ms). This drop is a suspected effect of some data acquisition issues.

- An effect on the signal is observed when the breakdown occurs and the plasma is created. A reaction to the presence of plasma is shown in figure 6.2.

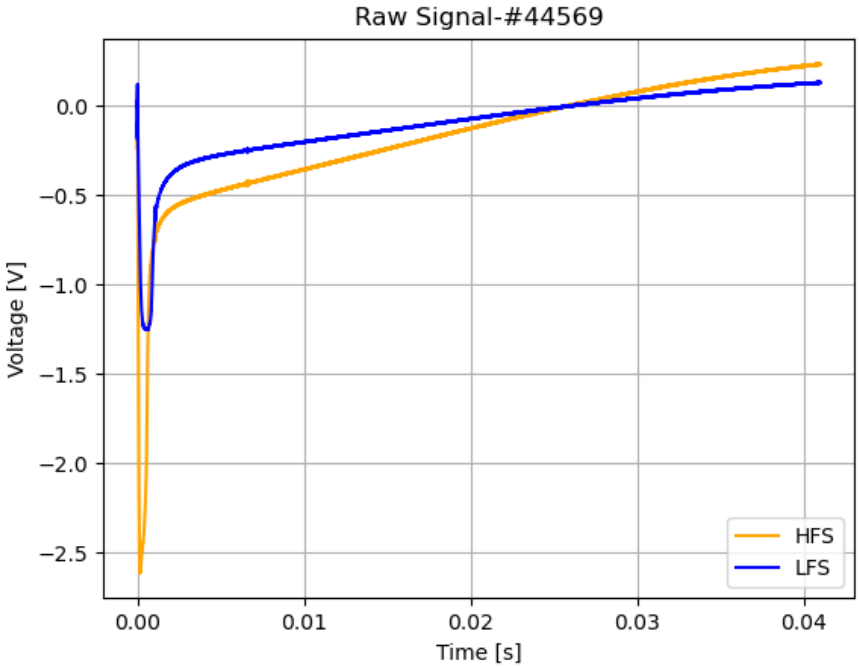

Figure 6.1: Raw signals from the toroidal field coils on the HFS and LFS for a vacuum shot for $UBt = 800$ V.

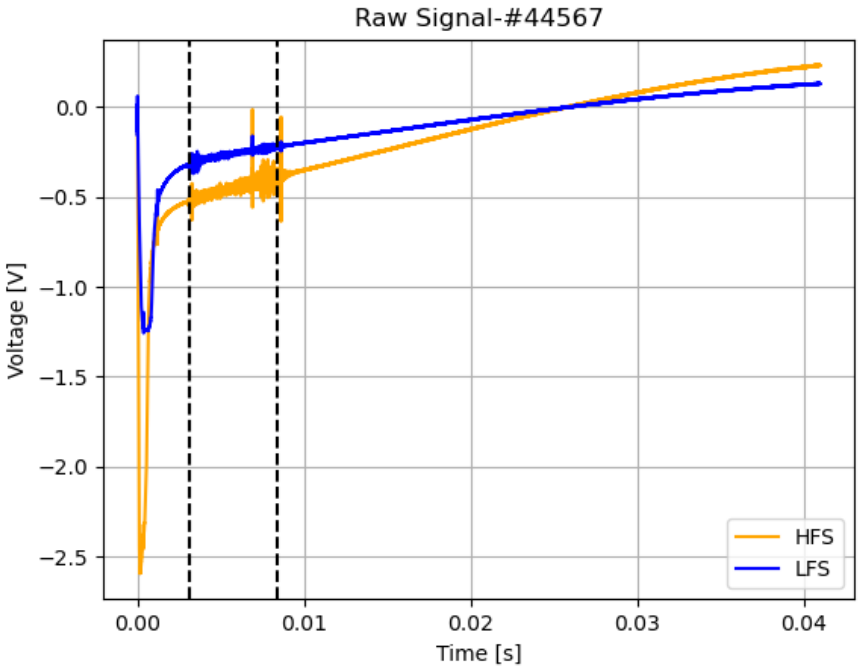

Figure 6.2: Raw signals from the toroidal field coils on the HFS and LFS for a plasma shot for $UBt = 800$ V. Vertical dashed lines depict plasma discharge.

6.2 Processing The Signals

The signals from the HFS and LFS coils are processed by integrating the equations 4.7 and 4.8. The result of the integration shows that the field on the high field side is greater than the field on the low field side (figures 6.3 and 6.4), as expected.

A steepness is observed in the integrated signals within 1 ms of discharging the capacitors activating UBt. This coincides with the sudden drop in the signal as pointed out in the observations of the previous section. This steepness is not physical, but a result of faulty electronics, and should be corrected for. To effect this correction, a fit slightly similar to that performed for the Rogowski coil is made in the next section.

Recall that the second observation about the raw signal in section 6.1 indicated a response to the presence of plasma. Yet, in the integrated signal, this response has no visible effect. The integrated signals on figures 6.3 and 6.4 are very similar, so there are no apparent differences between plasma measurements and vacuum measurements for these coils.
The magnitude of B_{tor} in both location confirms their designation. Maximum at HFS is approximately 0.52 T, higher than the maximum at the LFS, 0.32 T. This is elaborated in another section.

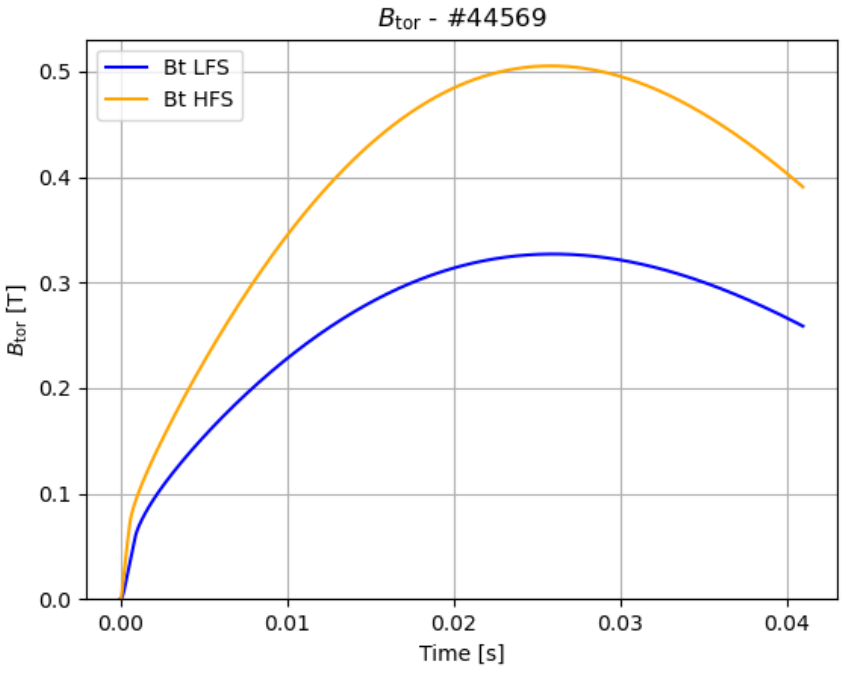

Figure 6.3: Integration of the raw signals of a vacuum shot

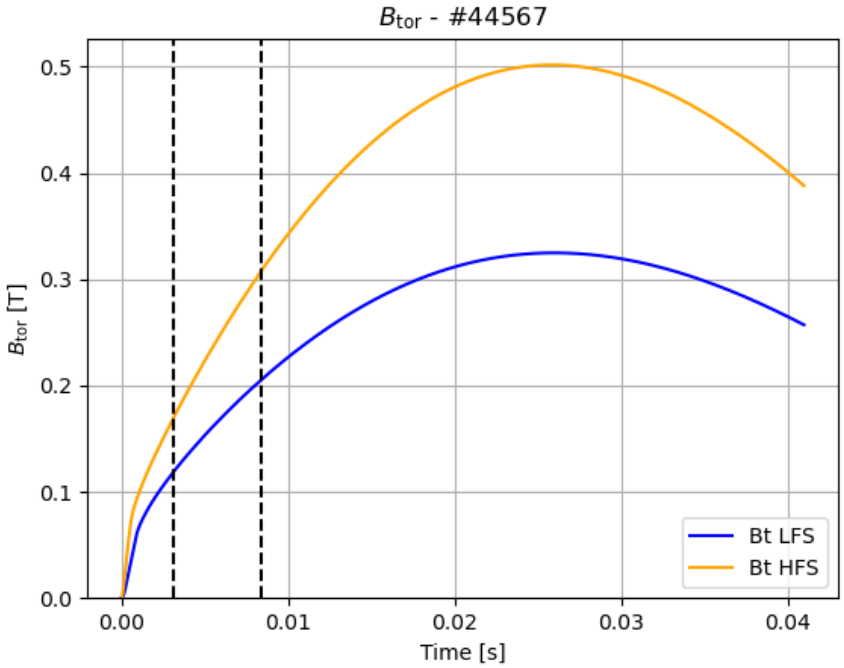

Figure 6.4: Integration of the raw signals of plasma shot.

6.3 Removing Steepness By B_{tor} Modelling

Understanding that the observed steepness within the 1 ms is an outcome of problems with the data acquisition system, the steepness is resolved.
To do this, part of the well behaved portion of the integrated signal (2 ms before and all data-points after breakdown) is modelled as an RLC circuit as in [11] but with a slight modification:

$$B_{tor} = \frac{\mu_0 N}{2\pi r} C U_0 \frac{\beta^2 + {\omega_0}^2}{\omega_0} e^{-\beta t} sin(\omega_0 t) + K. \tag{6.1}$$

Equation 6.1 is parameterized as:

$$B_{tor+offset} = \alpha_1 e^{-\alpha_2 t} sin(\alpha_3 t) + K, \tag{6.2}$$

with

$$\alpha_1 = \frac{\mu_0 N}{2\pi r} C U_0 \frac{\beta^2 + {\omega_0}^2}{\omega_0}, \tag{6.3}$$

$$\alpha_2 = \beta, \tag{6.4}$$

$$\alpha_3 = \omega_0. \tag{6.5}$$

K is added to the RLC function to account for the steepness. This offset is subtracted from the original data and and the remnant equals the accurate local toroidal magnetic field:

$$B_{tor} = B_{tor+offset} \; - \; K. \tag{6.6}$$

The results of the fit for both HFS and LFS are displayed in figures 6.5 and 6.6. Also the results after subtracting the offset, K for both the HFS and the LFS are shown in figures 6.7 and 6.8.

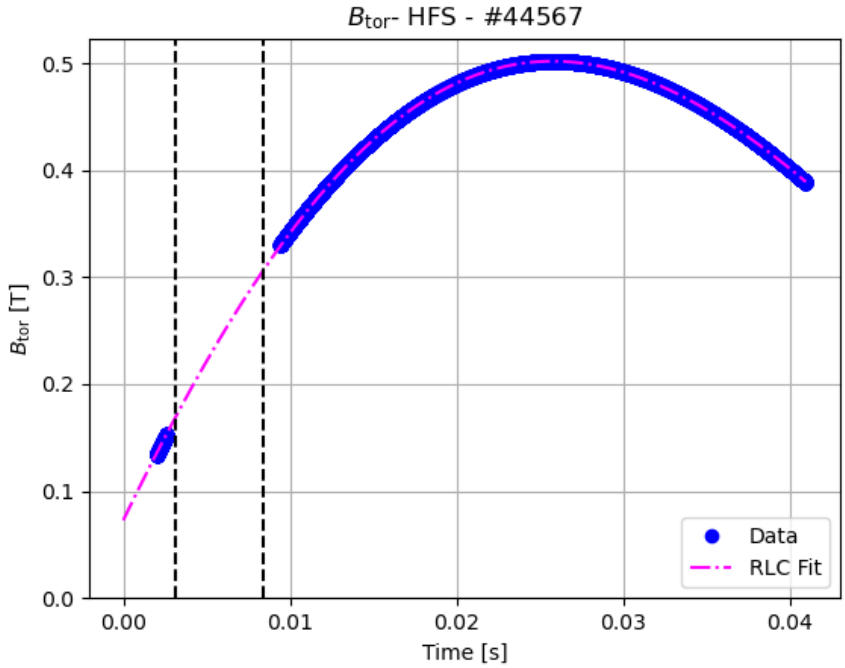

Figure 6.5: Fit performed and the result is $B_{HFS\ +\ offset} = 0.638e^{13.981t}sin(50.51t) + 0.073$. $K = 0.073$ *is the value at zero-crossing and represents the offset to be removed to account for the steepness.*

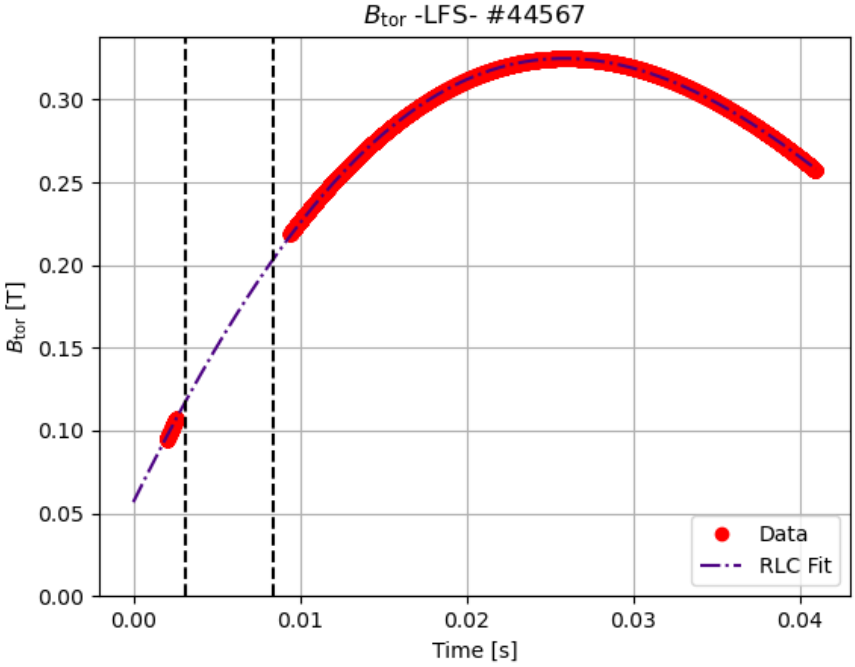

Figure 6.6: Fit performed with the result as $B_{LFS\ +\ offset} = 0.415e^{15.171t}sin(49.23t) + 0.057$. $K = 0.057$ *is the value at zero-crossing and represents the offset to be removed to account for steepness.*

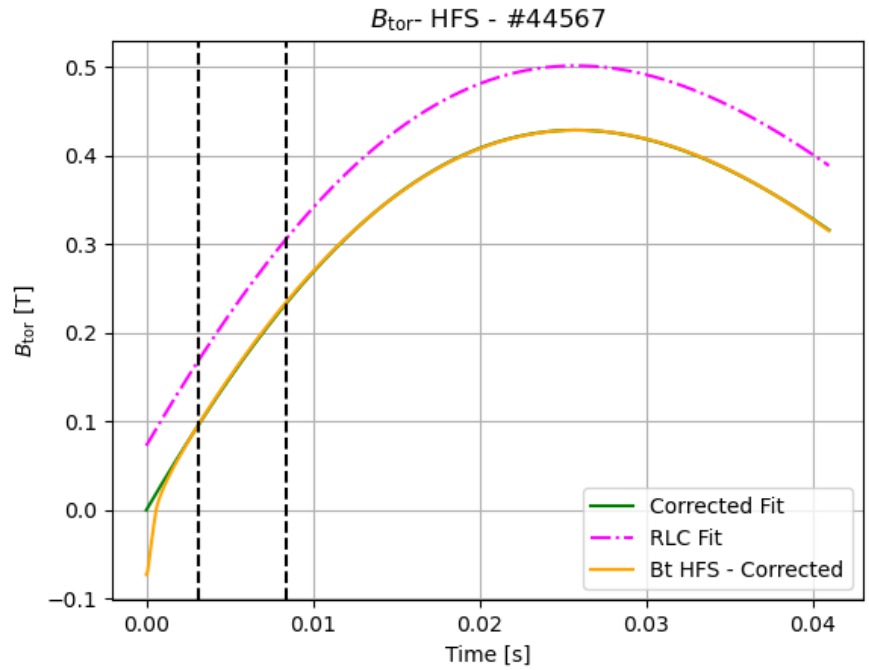

Figure 6.7: HFS B_{tor} after the correction is made with the RLC fit and steepness is accounted for.

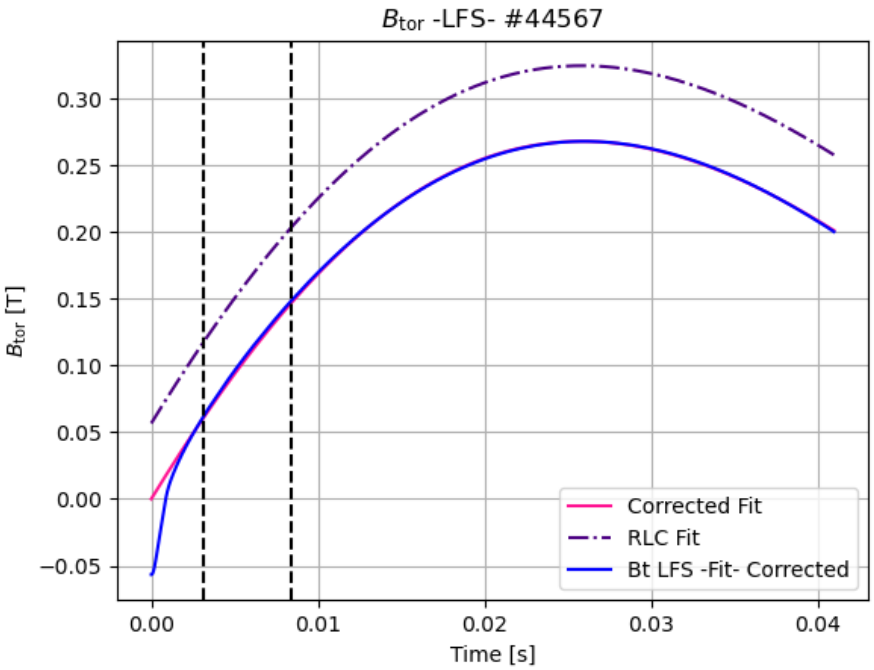

Figure 6.8: LFS B_{tor} after correction is made with the RLC fit and steepness is accounted for.

The capacitor was charged with different voltages, UB_t and shots were executed. The fit parameters for these shots are shown in the table 6.1.

Shot Number	UB_t [V]	HFS				LFS			
		α_1	α_2	α_3	K	α_1	α_2	α_3	K
44587	650	0.549	14.14	50.39	0.070	0.365	15.60	48.89	0.053
45586	700	0.570	14.08	50.44	0.071	0.378	15.38	49.06	0.054
45585	750	0.609	14.05	50.49	0.071	0.399	15.21	49.21	0.055
44604	750	0.568	13.96	50.50	0.071	0.375	15.27	49.09	0.054
44590	800	0.637	13.94	50.58	0.072	0.412	14.93	49.44	0.056
44606	850	0.670	13.91	50.60	0.073	0.430	14.75	49.58	0.057
44588	850	0.672	13.90	50.60	0.072	0.432	14.76	49.56	0.057
44592	900	0.702	13.87	50.64	0.073	0.448	14.61	49.70	0.058
44606	900	0.703	13.74	50.70	0.074	0.447	14.43	49.81	0.058
44594	1000	0.763	13.77	50.73	0.075	0.481	14.32	49.95	0.059

Table 6.1: Parameters obtained from the RLC fit on the local toroidal field coils measurements for different shots with different UB_t input.

6.4 Calibration of the Local Toroidal Field Coils

6.4.1 Local Mapping of B_{tor}

The hall probe was used to calibrate the HFS and LFS toroidal field coils. The probe was placed inside the tokamak on two different radial positions. It measured directly the local toroidal field due to its absolute calibration.

Measured values of B_{tor} were fitted with the expected $\frac{1}{R}$ - dependence of the B_{tor} on the radial position in the torus:

$$B_{tor}(R) = \frac{a}{R}, \tag{6.7}$$

where $a = 0.044046$ is the fit constant.

Finally, the values on the HFS ($R = 0.315$ m) and the LFS (0.485 m) were calculated as:

$$B_{tor}(HFS) = 0.140\ T, \tag{6.8}$$

$$B_{tor}(LFS) = 0.091\ T. \tag{6.9}$$

6.4.2 Obtaining Calibration Constants

The local toroidal field coils should measure the same fields as the Hall probes. The calibration constants are obtained using this condition:

$$0.140 = B_{tor-HFS} \times C_{HFS}, \tag{6.10}$$

$$0.091 = B_{tor-LFS} \times C_{LFS}. \tag{6.11}$$

The values measured by the local toroidal field coils are $B_{tor} = 0.08171$ T and $B_{tor} = 0.05931$ T. So the calibration constants are:

$$C_{HFS} = \frac{0.140}{0.08171} = 1.7134, \tag{6.12}$$

$$C_{LFS} = \frac{0.091}{0.05931} = 1.5343. \tag{6.13}$$

Multiplying the corrected fits of both HFS (green in figure 6.7) and LFS (purple in figure 6.8) by the newly obtained constants results in much more accurate local toroidal field measurements than by deducing the calibration factor from geometrical and physical properties of the coils. The example of the final B_{tor} signals after the calibration are shown in figure 6.9 with the signal of the outer B_{tor} coil for the comparison. A good agreement is evident, because the outer coil should be calibrated to measure toroidal magnetic field approximately in the middle of the chamber.

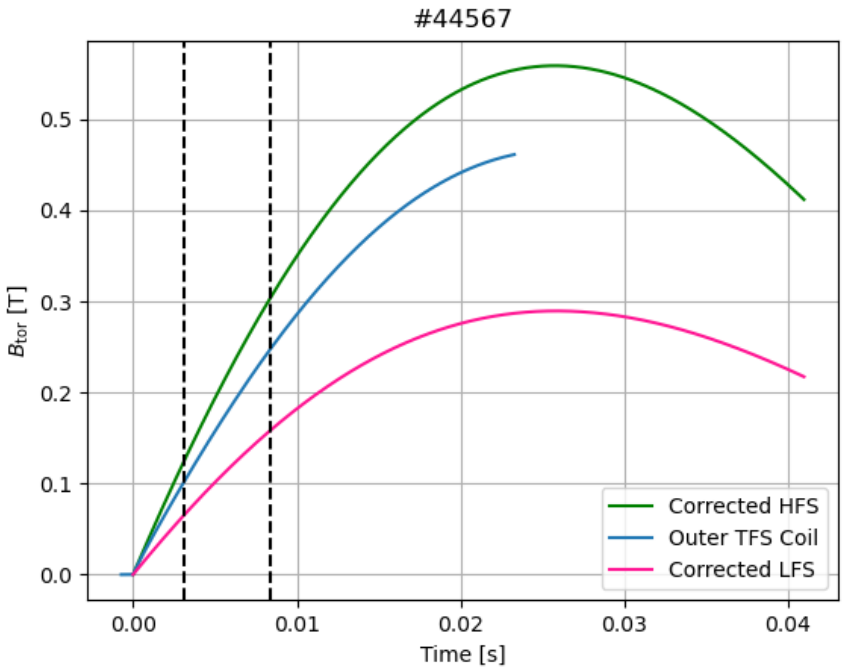

Figure 6.9: HFS (green) and LFS (purple) toroidal field measurements after calibration. Calibrations were done with Hall probes.

Chapter 7

Diamagnetic Loops Measurement

7.1 Raw Signals

The diamagnetic loops is one of the many different ways by which toroidal magnetic flux can be measured [[23],[24],[15], [25],[26] and [14]]. The diamagnetic loops detect voltage signals by induction just like the Rogowski coil and the toroidal magnetic field measuring coils. Figures 7.1 and 7.2 show the measured signals for a vacuum discharge and a plasma discharge, respectively. A visible activity is detected during plasma duration (2 ms - 13 ms) for the plasma shot as compared to the vacuum shot. The activity depends on the plasma current, density and temperature. The higher these plasma properties are, the higher the activity. The activity translates to a noticeable change in toroidal flux in the plasma. This quantity is the interest of this measurement.

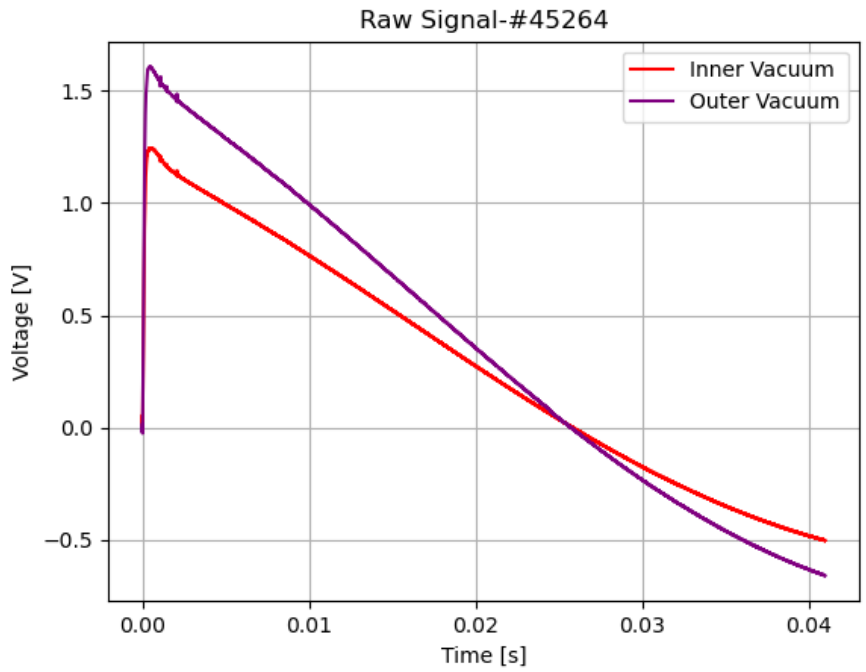

Figure 7.1: Raw signal from the inner and outer diamagnetic loops for a vacuum shot (#45624).

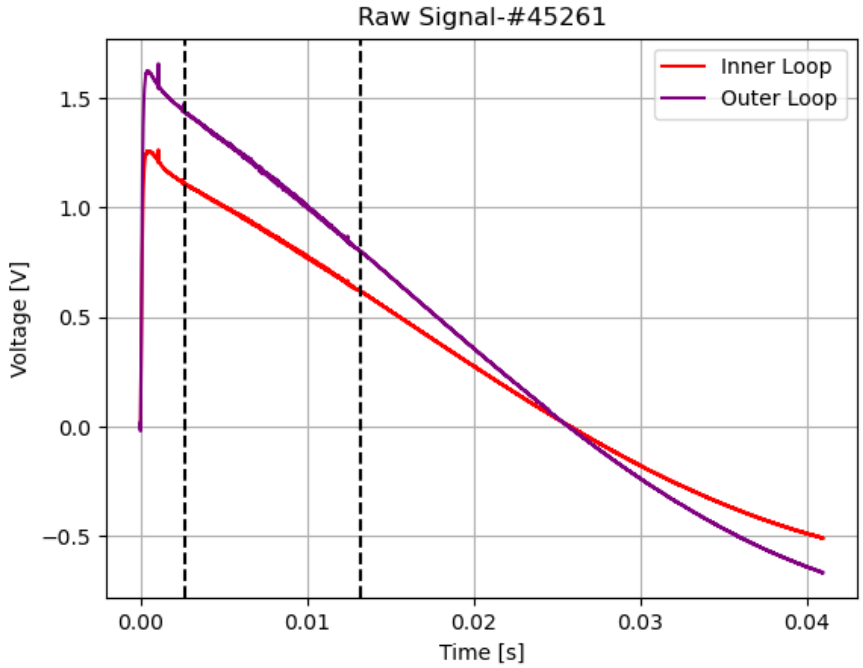

Figure 7.2: Raw signal from the inner and outer diamagnetic loops for a vacuum shot (#45621).

7.2 Compensation of Signals

The inner loop (diameter $= 175$ mm) encloses the plasma column as closely as possible to pick the flux of the plasma. The other loop being much wider obtains a maximum ratio of the areas out of the plasma measured by both loops. The inner loop is called the measuring loop while the outer loop is the compensation loop [14].
The principle of conservation of magnetic flux is applied for compensating vacuum magnetic field to the magnetic field in the presence of plasma. For a vacuum discharge,

$$U_1 = -A_{in}\frac{dB_0}{dt}, \tag{7.1}$$

$$U_2 = -A_{out}\frac{dB_0}{dt}. \tag{7.2}$$

U_1 and U_2 are the voltage signals from the inner and outer loops, A_{in} and A_{out} are the respective areas enclosed by the loops, while B_0 is the background toroidal magnetic field when there is no plasma.
In the presence of plasma, the magnetic field will be modified and the signals are [14]:

$$U_1 = -\pi a^2\frac{dB_i}{dt} - A_{in}\frac{dB_e}{dt} + \pi a^2\frac{dB_e}{dt}, \tag{7.3}$$

$$U_2 = -\pi a^2\frac{dB_i}{dt} - A_{out}\frac{dB_e}{dt} + \pi a^2\frac{dB_e}{dt}. \tag{7.4}$$

Here, a is the minor radius of the tokamak, B_i and B_e are the toroidal magnetic field associated with the inner and the external loops respectively.

The vacuum signals are used for amplitude matching to get both the same:

$$\Delta U = U_1 - mU_2 = -A_{in}\frac{dB_0}{dt} + mA_{out}\frac{dB_0}{dt} = 0, \tag{7.5}$$

with m as the matching factor of the signals. The compensated signal in the presence of plasma is:

$$\Delta U = U_1 - mU_2 = -m(\frac{A_{out}}{A_{in}} - 1)\frac{d}{dt}\Delta\Phi. \tag{7.6}$$

Figures 7.3 and 7.4 are the integrated signals in cases of vacuum and plasma discharges, respectively. A difference in the signals can be seen and this is matched using equation 7.5 and displayed in figure 7.5. The selected portion for the matching is bounded by the dashed lines.
$\Delta\Phi$ in equation 7.6 is the desired quantity for the further analysis.

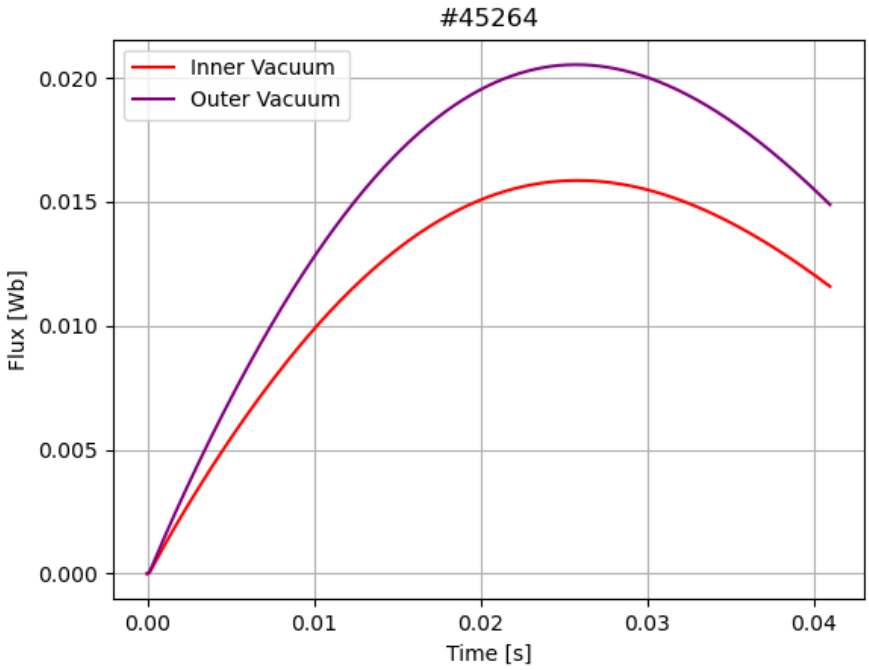

Figure 7.3: Integrated signals for the inner and the outer diamagnetic loops for a vacuum shot (#45264). These signals are used for the toroidal magnetic field compensation.

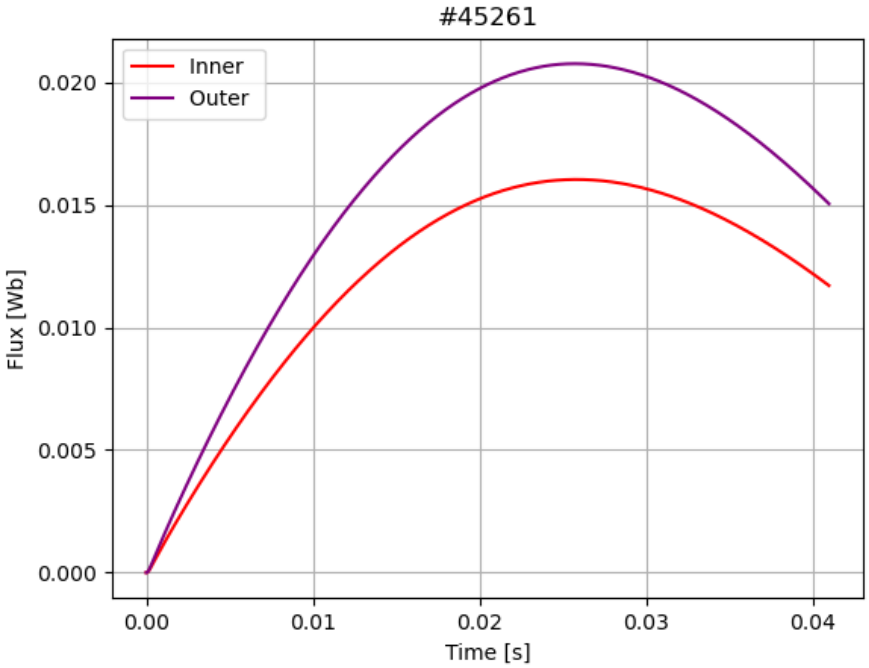

Figure 7.4: Integrated signals for the inner and the outer diamagnetic loops for a plasma shot (#45261).

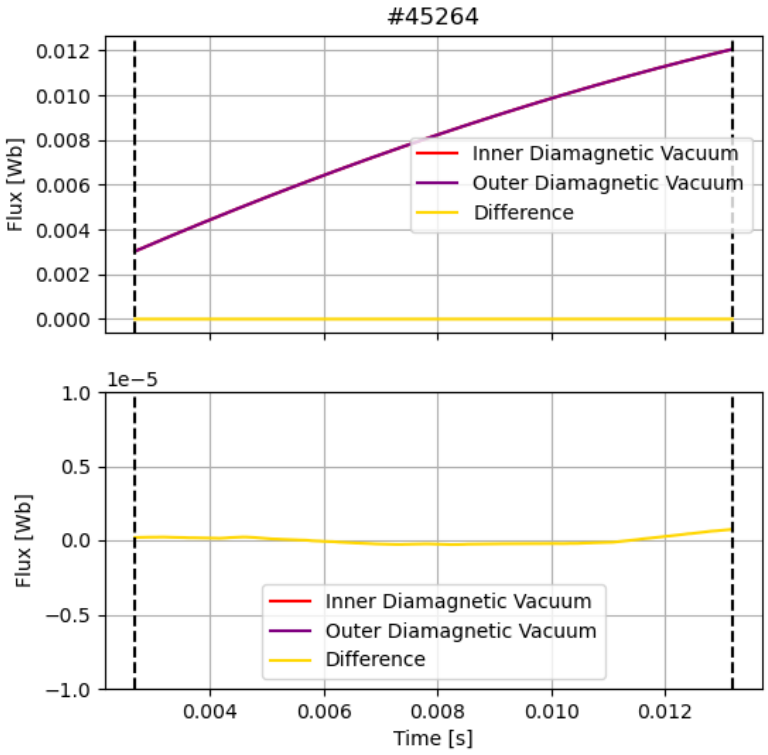

Figure 7.5: The signal matching of the inner and outer loop measurements (a). Matching is not perfect in regions near plasma endpoints as signal difference (yellow) is not zero when zoomed in (b).

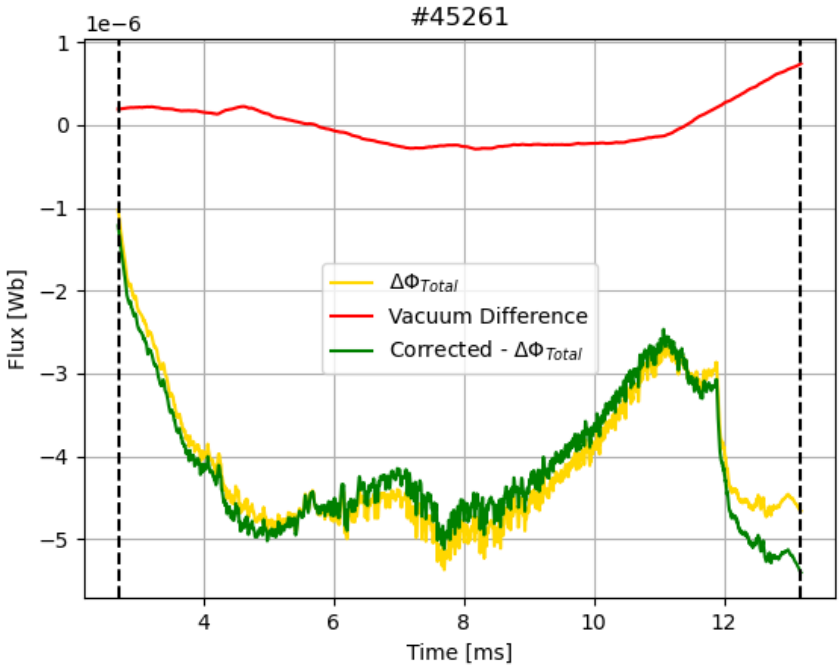

Figure 7.6: The magnetic flux derived from compensation (yellow), corrected (green) for inaccuracies in the vacuum signal matching (red).

7.3 Flux Contributions

The toroidal magnetic flux change for a plasma discharge ($\#45621$) after compensation is shown in figure 7.6. The original $\Delta\Phi_{Total}$ (yellow) is obtained from 7.6.
The matching of the vacuum signals is not perfect as seen from figure 7.6 (red). This residual is subtracted from the original (yellow), and a corrected $\Delta\Phi_{Total}$ (green) is obtained.

The change in toroidal flux is as a result of two effects of plasma - paramagnetic and diamagnetic contributions.
The paramagnetic contribution to the flux is a result of the plasma current I_p, and can be obtained from equation 2.18. Figure 7.7 shows this flux for a plasma discharge with current, $I_p > 5$ kA. A high current discharge is used because the plasma density and temperature is high in this regime. High density and temperature plasma have more impact in these kind of measurements.
In this calculation, the more accurate plasma current obtained from the new inner Rogowski coil discussed in chapter 5 has been used.
The paramagnetic flux, $\Delta\Phi_{paramagnetic} < 5 \cdot 10^{-6}$ has a maximum when the current is the highest (about 9 ms). At this point, the plasma conducts the most during the discharge.

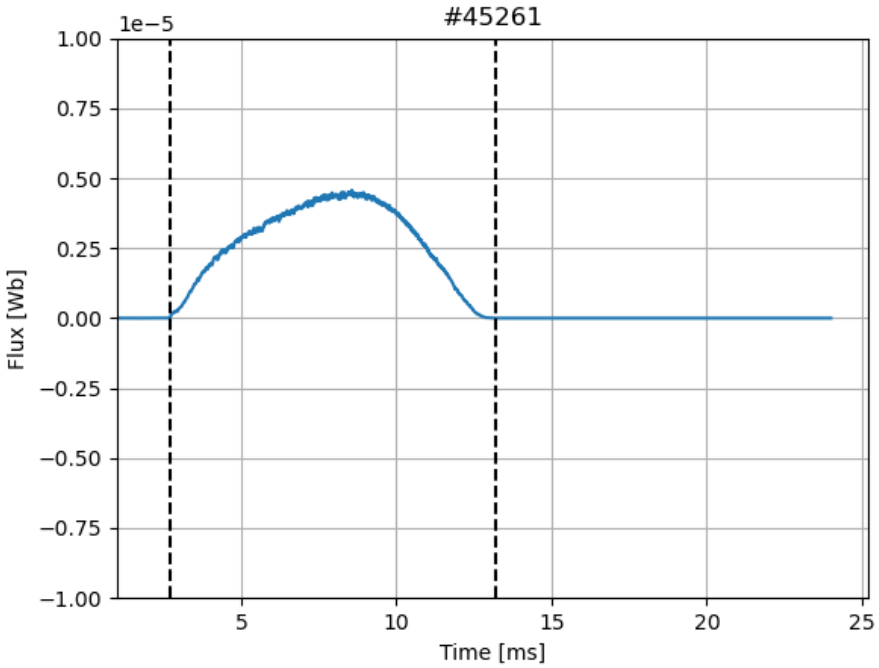

Figure 7.7: Paramagnetic flux ($\Delta\Phi_{paramagnetic} = \frac{(\mu_0 I_p)^2}{8\pi B_0}$) from the plasma current.

The second contribution is the diamagnetic flux from which the perpendicular energy is obtained. The diamagnetic flux is obtained by subtracting the paramagnetic flux from the total flux change. This result is shown in figure 7.8 where all fluxes have been plotted.
Diamagnetic contribution to the flux change is a consequence of the ion cyclotron movement in a plane perpendicular to magnetic field lines [14].

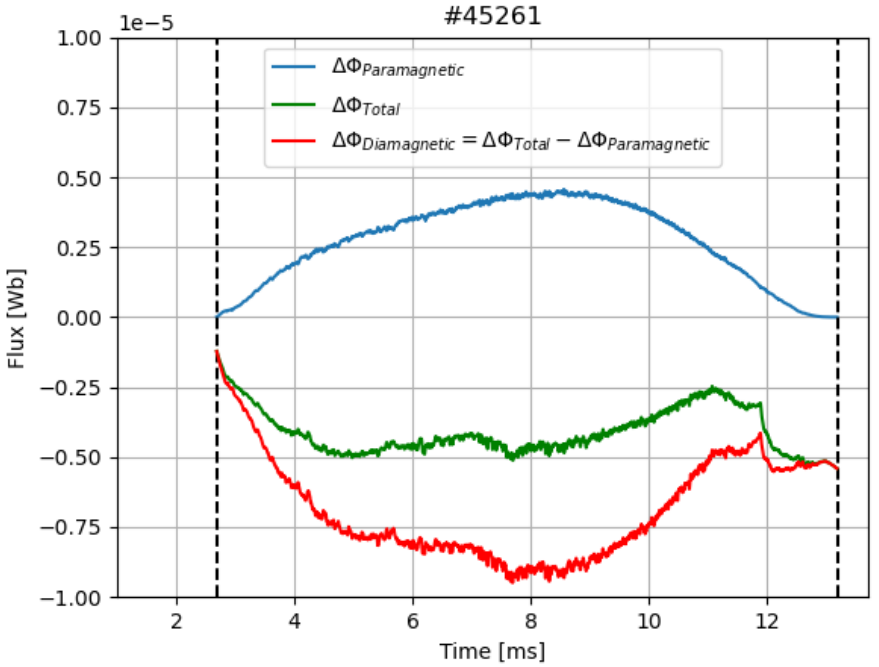

Figure 7.8: Total magnetic flux (green), paramagnetic flux (blue) and diamagnetic flux (red)

7.4 Perpendicular Energy, Thermal Energy, Power and Energy Confinement Time

The perpendicular energy component of the plasma column is obtained from the diamagnetic flux in the plasma cross-section [26]:

$$W_\perp = -\frac{B_0}{\mu_0}\Delta\Phi_{Diamagnetic}. \tag{7.7}$$

The result of this is shown in figure 7.9. The energy rises steadily as the plasma heats up and peaks around 9 ms at $W_\perp \approx 2.8$ [J/m]. At around this time, the plasma current also reaches maximum.

By the assumption of an isotropic Maxwellian distribution, the perpendicular energy is twice the parallel energy:

$$W_\perp = 2W_{||}, \tag{7.8}$$

such that the total kinetic energy is:

$$W = W_\perp + W_{||} = W_\perp + \frac{1}{2}W_\perp = \frac{3}{2}W_\perp. \tag{7.9}$$

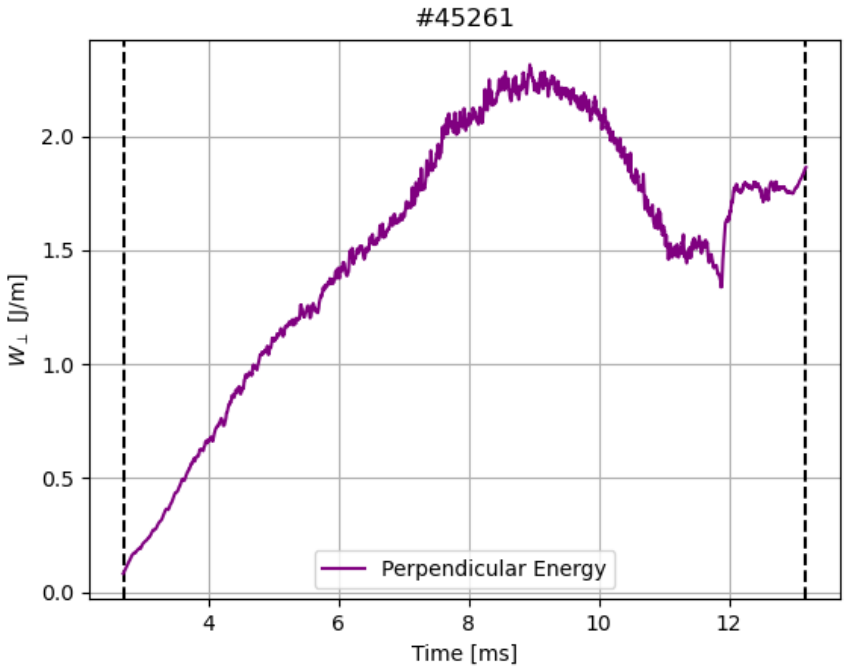

Figure 7.9: Perpendicular energy of the plasma obtained from the diamagnetic flux.

The total kinetic energy integrated over the cross-section results in the total plasma thermal energy:

$$W_{th} = \frac{3}{2}W_\perp \cdot 2\pi R, \tag{7.10}$$

where $R = 0.4$ m is the major radius of the GOLEM tokamak. This is contained in figure 7.10.

The total plasma thermal energy rises to a maximum value of over 20 J.
The energy confinement time, τ_E can be calculated over the time of the plasma discharge. From this we can see the time behaviour of the capacity of the plasma to contain its energy. This is evaluated for stationary discharge phase using the equation:

$$\tau_E = \frac{W_{th}}{P_\Omega}. \tag{7.11}$$

Here, P_Ω is the Ohmic heating power produced by the plasma current, I_p and the loop voltage, U_{loop}:

$$P_\Omega = I_p U_{loop}. \tag{7.12}$$

Figure 7.11 shows the Ohmic heating power. The power is determined by the current and as expected increases as the plasma grows, reaches the maximum around 70 kW and quickly ramps down as the plasma discharge ends.

The evaluated energy confinement time drops steadily over time during the plasma discharge and is in the order of fractions of milliseconds as seen in 7.12.
The results of the perpendicular energy component, the thermal energy and the energy confinement time of the plasma are in agreement with previous measurements in the CASTOR tokamak [26].

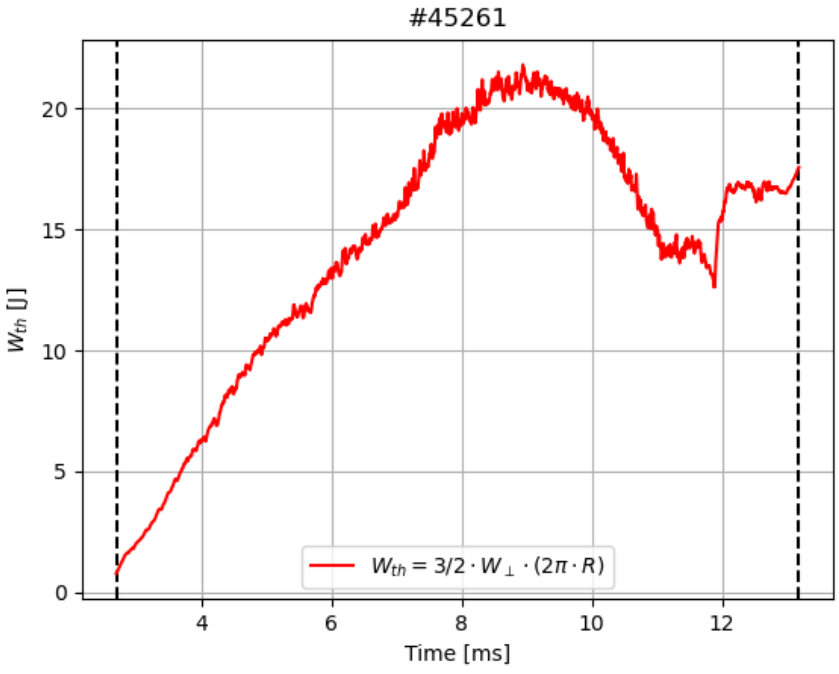

Figure 7.10: Total thermal energy of plasma. $W_{th} = \frac{3}{2} W_\perp \cdot 2\pi R$.

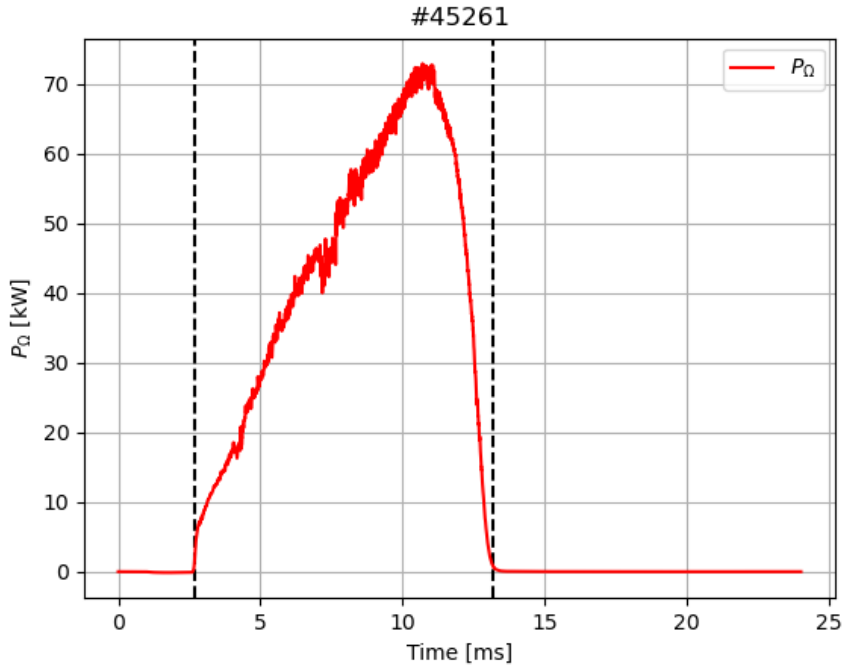

Figure 7.11: Ohmic heating power due to the plasma current.

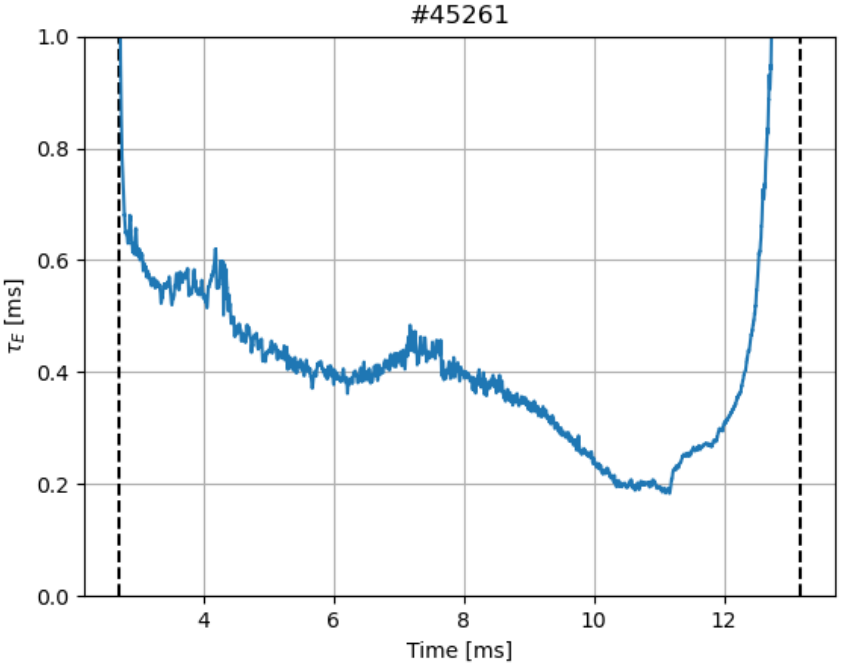

Figure 7.12: Time evolution of the energy confinement time evaluated from the thermal energy and the ohmic heating power.

Chapter 8

Conclusions and Future Work

A new set of magnetic coils has been designed to improve the accuracy of standard magnetic measurements and facilitate the measurement of the plasma thermal energy and the energy confinement time in the GOLEM tokamak. These two parameters require highly accurate measurements of plasma current and toroidal magnetic field which can be obtained by installing the coils inside the vacuum vessel.

The introductory chapter gives the motivation, aim and objectives of the thesis. The following chapter describes the theoretical framework giving an insight into thermonuclear fusion plasma. It presents magnetic confinement devices with a focus on the magnetic configuration. Special attention is given to the plasma diamagnetism.

The third chapter describes the GOLEM tokamak and its magnetic diagnostics: the discharge procedure, basic parameters, principle of magnetic measurements and coil designs. The fourth chapter describes the new inner diagnostics system.

The next two chapters elaborate the steps which lead to the main goal of the new diagnostics system. The fifth chapter describes the analyses of the new Rogowski coils. It compares the new inner Rogowski coil to the old one which has been used as one of the standard magnetic diagnostics. The signal was fitted to remove to toroidal magnetic field pick-up and the integration offset. Moreover, comparison of the outer and inner Rogowski coil enabled the modelling of the chamber current producing the values of the resistance and inductance of the chamber.

The sixth chapter focuses on the local toroidal magnetic field coils. The signal was analysed to obtain the toroidal field at the high field side and the low field side. The signals were fitted in order remove a parasitic artefact of the electronics. The signals were calibrated and compared to reference measurements of the toroidal magnetic field by Hall probes.

The plasma thermal energy and the energy confinement were finally calculated in the seventh chapter. Obtaining these two quantities required very precise measurement of the total toroidal magnetic flux. This was extremely difficult to accomplish as the paramagnetic and diamagnetic effect of the plasma are nearly the same and they almost cancel each other. Moreover, they are three to four orders smaller than the toroidal magnetic flux. The precise analysis given in the fifth and sixth chapters repay in this difficult task. The obtained results are in agreement with these parameters previously measured in the CASTOR tokamak [26].

The refined signals of the plasma current (Rogowski coil), the local toroidal magnetic field as well as the plasma thermal energy and energy confinement time have been included in the

shot web page of the GOLEM tokamak.

The thesis presents first results and calibration of the new system of inner magnetic coils. It proves that the system is viable. Further work would include testing of the system in different plasma regimes and tokamak condition. The main focus will be on improving the compensation of the diamagnetic coils.

Bibliography

[1] O. Grover, J. Kocman, M. Odstrcil, T. Odstrcil, M. Matusu, J. Stockel, V. Svoboda, G. Vondrasek, and J. Zara. Remote operation of the GOLEM tokamak for fusion education. *Fusion Engineering and Design*, **112** (2016) 1038–1044. ISSN 0920-3796

[2] Website of the GOLEM tokamak. `https://www.golem.fjfi.cvut.cz/`, 2024. Accessed in June, 2024.

[3] T. Markovic. *Measurements of Magnetic Fields on GOLEM Tokamak*. Ph.D. thesis, Czech Technical University in Prague, Prague, 2012

[4] E. Rutherford. Collision of particles with light atoms.An anomalous effect in nitrogen. *The London, Edinburgh, and Dublin Philosophical Magazine and Journal of Science*, **37** (1919) (222) 581–587. ISSN 1941-5982, 1941-5990. URL `http://dx.doi.org/10.1080/14786440608635919`

[5] F. W. Aston. Isotopes and Atomic Weights. *Nature*, **105** (1920) (2646) 617–619. ISSN 0028-0836, 1476-4687. URL `http://dx.doi.org/10.1038/105617a0`

[6] A. S. Eddington. *Space, time and gravitation: an outline of the general relativity theory*. Cambridge science classics. Cambridge university press, Cambridge (GB) New York Port Chester [etc.], new ed. edition, 1990. ISBN 978-0-521-33709-0

[7] C. F. Weizsäcker. "Über Elementumwandlungen im Innern der Sterne. I" (On transformations of elements in the interiors of stars. I). *Physikalische Zeitschrift (Physics Journal)*, **38** (1937) 176–191

[8] C. F. Weizsäcker. "Über Elementumwandlungen im Innern der Sterne. II" (On transformations of elements in the interiors of stars. II). **39** (1938) 633–646

[9] H. A. Bethe. Energy Production in Stars. *Physical Review*, **55** (1939) (5) 434–456. ISSN 0031-899X. URL `http://dx.doi.org/10.1103/PhysRev.55.434`

[10] F. F. Chen. *Introduction to Plasma Physics and Controlled Fusion*. Springer, Switzerland, 3. ed edition, 2002. ISBN 978-3-319-22309-4 (eBook)

[11] J. Brotankova. *Study of High Temperature Plasma in Tokamak-Like Experimental Devices*. Ph.D. thesis, Institute of Plasma Physics, Prague, 2009

[12] S. Li, H. Jiang, Z. Ren, and C. Xu. Optimal Tracking for a Divergent-Type Parabolic PDE System in Current Profile Control. *Abstract and Applied Analysis*, **2014** (2014) e940965. ISSN 1085-3375. Publisher: Hindawi, URL `http://dx.doi.org/10.1155/2014/940965`

[13] L. Lao, H. St. John, R. Stambaugh, A. Kellman, and W. Pfeiffer. Reconstruction of current profile parameters and plasma shapes in tokamaks. *Nuclear Fusion*, **25** (1985) (11) 1611–1622. ISSN 0029-5515, 1741-4326. URL http://dx.doi.org/10.1088/0029-5515/25/11/007

[14] F. Zacek and L. Kryska. Evaluation of perpendicular energy component from changes of parallel magnnetic flux. *Technical report*, Ustav fyziky plazmatu CSAV, 1980

[15] V. Pustovitov. Extended theory of diamagnetic measurements with account of the wall currents in tokamaks. *Fusion Engineering and Design*, **138** (2019) 53–58. ISSN 09203796. URL http://dx.doi.org/10.1016/j.fusengdes.2018.11.001

[16] V. Svoboda, G. Pokol, D. I. Réfy, J. Stockel, and G. Vondrášek. Former tokamak CASTOR becomes remotely controllable GOLEM at the Czech Technical University in Prague. (2023)

[17] V. Svoboda, A. Dvornova, R. Dejarnac, M. Prochazka, S. Zaprianov, R. Akhmethanov, M. Bogdanova, M. Dimitrova, Z. Dimitrov, O. Grover, L. Hlavata, K. Ivanov, K. Kruglov, P. Marinova, P. Masherov, A. Mogulkin, J. Mlynář, J. Stockel, and A. Volynets. Remote operation of the GOLEM tokamak with hydrogen and helium plasmas. *Journal of Physics: Conference Series*, **768** (2016) 012002. URL http://dx.doi.org/10.1088/1742-6596/768/1/012002

[18] S. Abbasi, J. Chlum, J. Mlynar, V. Svoboda, J. Svoboda, and J. Brotankova. Plasma diagnostics using fast cameras at the GOLEM tokamak. *Fusion Engineering and Design*, **193** (2023) 113647. ISSN 09203796. URL http://dx.doi.org/10.1016/j.fusengdes.2023.113647

[19] S. Tumanski. Induction coil sensors—a review. *Measurement Science and Technology*, **18** (2007) (3) R31–R46. ISSN 0957-0233, 1361-6501. URL http://dx.doi.org/10.1088/0957-0233/18/3/R01

[20] I. H. Hutchinson. *Principles of plasma diagnostics*. Cambridge University Press, Cambridge, 2. ed edition, 2002. ISBN 978-0-521-80389-2 978-0-521-67574-1

[21] A. Piel. *Plasma Physics: An Introduction to Laboratory, Space, and Fusion Plasmas*. Springer, Berlin, Heidelberg, 2010. ISBN 978-3-642-10490-9 978-3-642-10491-6. URL http://dx.doi.org/10.1007/978-3-642-10491-6

[22] C. McClenahan. A tutorial on Rogowski coil theory and operation. *Technical Report SAND-87-0043, 6379900, ON: DE88000006*, 1987. URL http://dx.doi.org/10.2172/6379900

[23] E. Joffrin and P. Defrasne. Differential method for the real time measurement of the diamagnetic and internal inductance in Tore Supra. *Review of Scientific Instruments*, **73** (2002) (6) 2266–2269. ISSN 0034-6748, 1089-7623. URL http://dx.doi.org/10.1063/1.1475350

[24] L. Giannone, R. Fischer, A. Kappatou, G. Tardini, M. Weiland, C. Angioni, E. Fable, M. Griener, R. McDermott, B. Sieglin, A. Jansen Van Vuuren, R. Bilato, M. Dunne, A. Gude, A. Kallenbach, J. Kurz, M. Maraschek, D. Rittich, F. Ryter, P. Schneider, K. Schuhbeck, U. Stroth, H. Zohm, and The Asdex Upgrade Team. Measurements and modelling of diamagnetic flux in ASDEX Upgrade. *Nuclear Fusion*, **61** (2021) (6) 066021. ISSN 0029-5515, 1741-4326. URL http://dx.doi.org/10.1088/1741-4326/abea56

[25] B. Shen, B. Wan, and X. Zhang. Diamagnetic measurement on HT-7 superconducting tokamak. *Fusion Engineering and Design*, **70** (2004) (4) 311–318. ISSN 09203796. URL `http://dx.doi.org/10.1016/j.fusengdes.2004.07.018`

[26] J. Brotankova, K. Jakubka, L. Kryska, J. Stockel, and F. Zacek. Measurement of energy confinement in CASTOR tokamak regimes with edge plasma polarization. *Czech Journal of Physics*, **50** (2000) 75–80

Acknowledgements

I begin by appreciating my supervisor, Jana Brotánková for the kind and exceptional guidance during this research. She supported the advancement of this work from the first day and her advice and support in my academics, career and social life are invaluable. Her attention to details and desire for excellence is very worthy of emulation and I am glad to be her student. Thank you for your understanding and your readiness to answer my many questions and listen to my painfully boring explanations.

I also appreciate the entire Fusion EP consortium for this great opportunity of attaining scholarship. Special thanks to Peter Beyer, Remy Guirlet and Carsten Lechte, for the sufficient guidance during this masters program. I must also appreciate Ondrej Ficker, who since the passing of Jan Mlynar (of blessed memory), has been very helpful in giving career advice as well as opinions about my research. To all the professors who taught me during this program, I show gratitude. I reserve special appreciation to Alf Kohn-Seemann, whose lectures on fusion research remains an asset to me. I also appreciate his advice and support to me.

For sure, I have to appreciate the enormous help I received from the technicians, researchers and students who worked with me at the GOLEM tokamak. Vojtech Svoboda was always interested in my work and was always available to put the tokamak in good conditions for my shots. For this, I really express my gratitude. Also, I can not forget the invaluable assistance of Lukas Lobko who assisted me all the way. His insights on experiments, analysis and interpretation of the results were very vital. I must mention the help of Daniela Koprackova and Marek Tunkl who were involved with the Hall probe measurements for calibrating the toroidal field measuring coils. Marek also photographed the diagnostics when already installed in the tokamak. I appreciate Tomas Markovic for his willingness to answer my questions.

It is important that I appreciate my colleagues in the Fusion EP for the great collaboration during the events and joint practicum. I have learned a lot from research conversations which we have had. Special recognition must go to my good friend, Federico Coto-Vilchez, who has been a reliable colleague in discussion of results and have been a great companion. I must also appreciate Abha and Rajbir, for their support.

Much love and appreciation to my parents who raised me and sponsored my education until this scholarship. It has not always been easy but they are always unwavering in their support in all ramifications. I am glad to see them celebrate me. I appreciate my siblings, Ogochukwu, Arinze, Chibuzor and Uchechukwu. The prayers and emotional support from my family are invaluable.

I must mention also my mentors, great friends and loved ones such as Ebube, Dinma, Assumpta, Emmanuel, Adonai, Goodness, Chidera, Delight, Chukwudi, Luis, Toby, Rukayat and Neme C, for their emotional support, love and care. Much appreciation to C^4, my choir back in Nigeria and my choir here in Prague for the melodious songs which helped me recharge after the stress of working in the lab. I appreciate the Erasmus scholars of Nigerian origin. I also think that the people who were sources of frustration and difficulty deserve appreciation for creating a balance in my mental state and helping me appreciate the great importance of those who do otherwise.

Finally, I appreciate myself for having the faith and resilience to complete this thesis, as well as to God for his grace and favour.

List of Tables

List of Figures

Declaration in lieu of oath

I am aware that plagiarism is not consistent with academic and research ethics. I declare in lieu of oath that all the work presented in this report, which is not cited in the text or by references, is my own work.

Prague, Czech Republic, June 25, 2024.

Godsfavour Chibueze Amanekwe

Copyright Agreement

I hereby grant the FUSION-EP consortium the non-exclusive right to publish this work.

I declare that this work is free of copyright claims of third parties.

Prague, Czech Republic, June 25, 2024.

Godsfavour Chibueze Amanekwe